UNITED NATIONS UNIVERSITY
GEOTHERMAL TRAINING PROGRAMME
Orkustofnun, Grensasvegur 9,
IS-108 Reykjavik, Iceland

Reports 2013
Number 9

DIRECT USE OF GEOTHERMAL ENERGY IN MENENGAI, KENYA: PROPOSED GEOTHERMAL SPA AND CROP DRYING

Samuel Kinyanjui
Geothermal Development Company
P.O. Box 100746 Nairobi 00101
KENYA
skinyanjui@gdc.co.ke, samuelkinyanjui@gmail.com

ABSTRACT

Direct use of geothermal heat as an energy source has significant economic and environmental benefits. Its use increases the utilisation efficiency of geothermal resources compared to electricity generation only. The use of geothermal heat in Menengai, Kenya, for bathing and drying of agricultural crops is proposed is this report. A geothermal spa of 2800 m^2 in water surface area, requiring 35 kg/s of geothermal flow is designed. Three location scenarios of the lagoon in Menengai field are evaluated with regard to pipeline cost. Conventionally heated swimming pools including an outdoor pool, indoor pool, steam room, wading pool and three hot tubs with a total water surface of 700 m^2 utilising 55 kg/s of 130°C geothermal fluid are analysed.

Utilisation of geothermal heat for drying is demonstrated through the design of a 30 m^3 mobile grain crop dryer comprised of a drying chamber, water-air heat exchanger and a blower. For air re-circulation purposes, a diversion valve from the tunnel to the bed dryer is provided for. The dryer requires 2 kg/s of 130°C geothermal water and has a capacity of 3 ton/hr of grains.

1. INTRODUCTION

Direct use of geothermal hot water as an energy source has significant economic and greenhouse gas emission benefits and also reduces the demand for electricity. Geothermal heat has been utilized since ancient times, mainly for bathing purposes. In Kenya, direct use has been on a relatively small scale, primarily in heating greenhouses, crop drying and bathing. In recent years, the government of Kenya has given more priority to the development of the geothermal resources in Kenya, and Menengai is one of the fields under development.

Menengai geothermal field is a high-temperature field located along the Kenya Rift valley, north of Lake Nakuru and south of Lake Bogoria. The Geothermal Development Company (GDC) has been carrying out drilling activities in the field and the first well, MW-01, successfully discharged in May 2011. The field is characterised by an elliptical caldera of 11.5 km in major axis (Kipng'ok, 2012), mainly covered by volcanic rocks which erupted from centres associated with the Menengai volcano. The field is in Nakuru, the fourth largest town in Kenya and a major agricultural centre in the country.

The agricultural sector is the largest contributor to the country´s GDP. It accounts for 24% of the country´s GDP (FAO, 2011) with seventy five per cent of the population directly or indirectly employed in this sector (Government of the Republic of Kenya, 2013). The food crops subsector contributes up to 32% of the agricultural GDP, with maize crops contributing about 15%. The other subsectors are industrial crops, horticulture, livestock and fisheries. Sixty five per cent of the total agricultural export is coffee and tea as the principal exports (KNBS, 2008). Flowers and horticultural products are also important foreign exchange income.

Drying of maize, tea and vegetables is done for storage purposes. The government of Kenya, through the National Cereals and Produce Board in Nakuru, dries maize in silo bins using diesel while tea is dried in major tea factories using wood or diesel. Coffee seeds have been majorly dried in the sun.

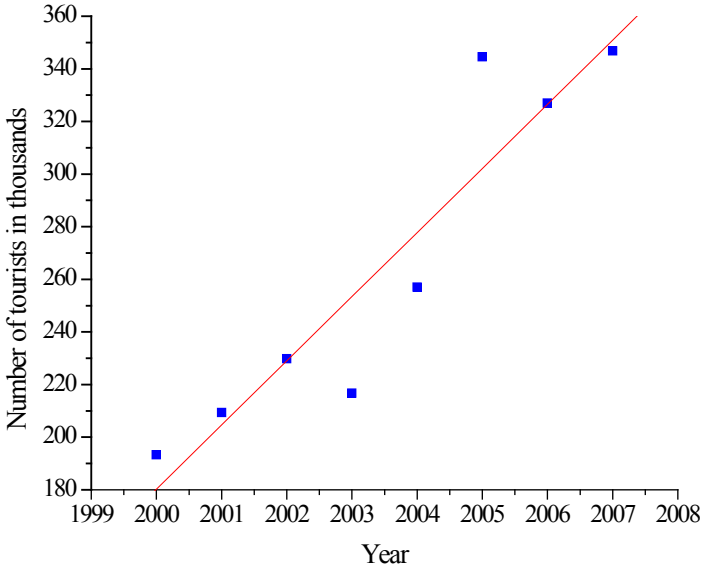

FIGURE 1: Tourists visiting Lake Nakuru
(Source: Ministry of tourism, 2010)

Tourism is the third largest contributor to the country's GDP after agriculture and manufacturing, providing 10% of the country's GDP (KNBS, 2008). The main tourist attractions are the country's world renowned national parks and beaches. Lake Nakuru, which is near Menengai geothermal field, is also a major tourist site, hosting over 300,000 foreign tourists annually, as shown in Figure 1.

Menengai caldera and Lake Nakuru National Park are the major tourist attraction sites in Nakuru County. The caldera peak offers a panoramic view of the surrounding areas including Nakuru Town. Lake Nakuru, a Ramsar site, located a few kilometres south of the Caldera, is famous for being the first successful Rhino Sanctuary in Kenya and a habitat for flamingos. There is a potential to package Lake Nakuru National Park together with the Menengai caldera and Lord Egerton Fort as tourist attraction sites under an ecotourism project. Menengai caldera is already attracting many local and foreign non-paying visitors.

The possibilities for direct utilization around Menengai are diverse and depend to a large extent on the economic activities in the area. Crop drying and bathing are some of the potential applications.

The aim of this project is twofold:

1) To propose a design for a geothermal spa in Menengai; and
2) To evaluate the use of geothermal heat in drying agricultural crops and to design a pilot grain dryer.

2. GEOTHERMAL SPAS AND SWIMMING POOLS

2.1 Background

Bathing is one of the earliest known uses of geothermal heat. Bathing in geothermal water is not only known to be a recreational activity today, but has therapeutic effects on the human body. Relaxation and stress relief, cleansing, socialization and musculoskeletal disorders are among the many factors as

to why millions of people around the world visit and enjoy the benefits of hot water in spas. Apart from offering these benefits, the spa is also a viable business venture.

Other health benefits derived from bathing in geothermal water include treatment of high blood pressure, skin diseases, diseases of the nervous system and relieving the symptoms of rheumatism. The mineral composition of geothermal waters, especially silica, has also been proven to have considerable healing effects for psoriasis skin disease (Pétursdóttir and Kristjánsson, 1995). Different guests visit and take baths in public bathing places and meet others from different quotas, hence enriching their social lives.

Steam baths and saunas have also been designed to utilize geothermal fluids. Relaxing in these facilities is associated with enormous health benefits including:

- Improved blood circulation;
- Cleaning and rejuvenating the skin;
- Eased muscle tension;
- Promotes feeling of relaxation and well-being; and
- Enhances detoxification processes.

The use of geothermal energy to heat swimming pools is a common practice, especially in cold countries such as Iceland where over 90% of the swimming pools are geothermally heated all year round (Orkustofnun, 2013).

2.2 Icelandic Blue Lagoon and Olkaria geothermal spa

The Icelandic Blue Lagoon, located in Svartsengi geothermal field, has an average temperature of 37°C, pH 7.5 and about 2.5% salinity (Pétursdóttir and Kristjánsson, 1995). It was gradually formed as an accident from disposed geothermal water. Currently, it gets the geothermal water from reservoirs with temperatures of 240°C in Svartsengi geothermal field, composed of 65% sea water and 35% fresh water (Ólafsson and Sigurgeirsson, 2003). The lagoon covers a water surface area of 4000 m^2 and the brine at 150°C flows at a rate of 40 l/s. It has a health clinic and, in total, the lagoon receives over 500,000 guests a year (internal communication).

In Olkaria field, a recently constructed geothermal spa utilises brine from a re-injection pipeline. It is comprised of two interconnected lagoons for cooling and flow regulation, a main bathing lagoon, 70 m in diameter, and a fourth children's pond, 10 m wide. The brine temperature is maintained at 30-35°C (Mangi, 2012) in the bathing pond.

The Mývatn baths in north Iceland utilise geothermal water from shallow wells. The water is cooled in a tank and then flows by gravity to the bathing lagoon. The temperature is regulated and maintained at 37°C. The baths cover a surface area of 2000 m^2 and are supplied by hot geothermal water at 15-20 l/s.

2.3 Proposed geothermal spa in Menengai

2.3.1 Source of geothermal water

The source of geothermal water for bathing in the spa is considered to be Well MW-03 which has a low wellhead pressure and a flow rate of 16 kg/s (GDC, 2013). Utilizing brine from Well MW-01 is also a possibility or from central separators in the future.

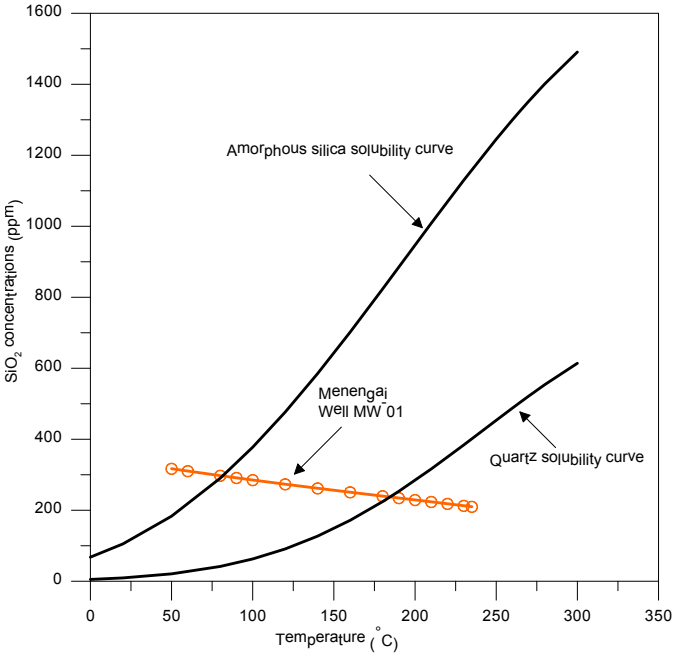

FIGURE 2: Silica concentrations in Well MW-01 during one step adiabatic boiling (Kipng'ok, 2011)

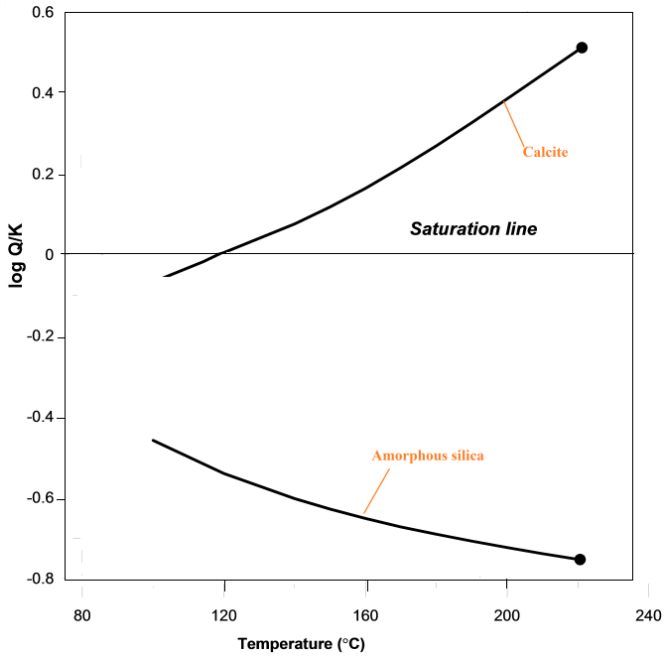

FIGURE 3: Calcite and amorphous silica saturation state during one step adiabatic boiling of Well MW-03 (GDC, 2013)

2.3.2 Silica scaling

Silica scaling is a universal challenge in the exploitation of geothermal fields producing brines and has largely inhibited the use of waste heat from discharge waters in these fields (Jamieson, 1984).

The solubility of silica decreases with a decrease in temperature. As opposed to carbonate, silica deposition is controlled by kinetics and can begin on the surface in several minutes or hours after reaching super saturation (Kashpura and Potapov, 2000). Similarly, silica scales are harder to remove mechanically.

Results based on Well MW-01 (Kipng'ok, 2011) indicate that amorphous silica precipitation will not occur until it is cooled below 88°C (Figure 2). If the temperature of the transported brine in the pipeline is maintained above this amorphous silica saturation temperature, then problems of silica scaling are avoided.

Analysis done on Well MW-03 (GDC, 2013) indicate that the water is under saturated with respect to amorphous silica even at lower temperatures, and there is no calcite scaling for temperatures below 120°C (Figure 3). Chemical analyses for Well MW-03, carried out in October 2012 at ambient temperature, indicate a fluid pH of 8.6 and a silica concentration of 362 mg/kg (Table 1).

Calcite deposition is predicted to occur, in minimal amounts only, according to chemical analysis and interpretation done on Well MW-03 (GDC, 2013).

2.3.3 Location of the geothermal spa in the field

Three location scenarios for the spa in Menengai field are considered in this report, as shown in Figure 4: locations A, B and C. The hot water delivery pipeline, cooling pond, main bathing pond and the pumping pond are designed for the three scenarios. The pipeline design and pumping for both the brine supply and the re-injection pipelines are evaluated for the different scenarios.

The sizes of the ponds are the same for all three scenarios.

The assumptions made are:

- The source of the geothermal fluid is assumed to be from Well MW-03 and no pumping will be required to supply the geothermal water to the spa;
- For all the scenarios, the re-injection point is near Well MW-02; and
- The cost of the pipes used is estimated from prevailing market prices in Kenya.

TABLE 1: Chemicals results for Well MW-03 carried out in October 2013 at 20°C (GDC, 2013)

Parameter	Value	Unit
pH	8.6	
SiO_2	362	mg/kg
TDS	6580	ppm
WHP	0.7	bar-g

Scenario A:
The spa is located at point A (Figure 4). This is approximately 3 km from the cold water pump site, near the main entrance to the field. The proposal for this location is based on the fact that this is close to the main entrance and, therefore, convenient for visitors to the spa. The area is fairly flat and has ample space to accommodate the bathing facilities envisaged.

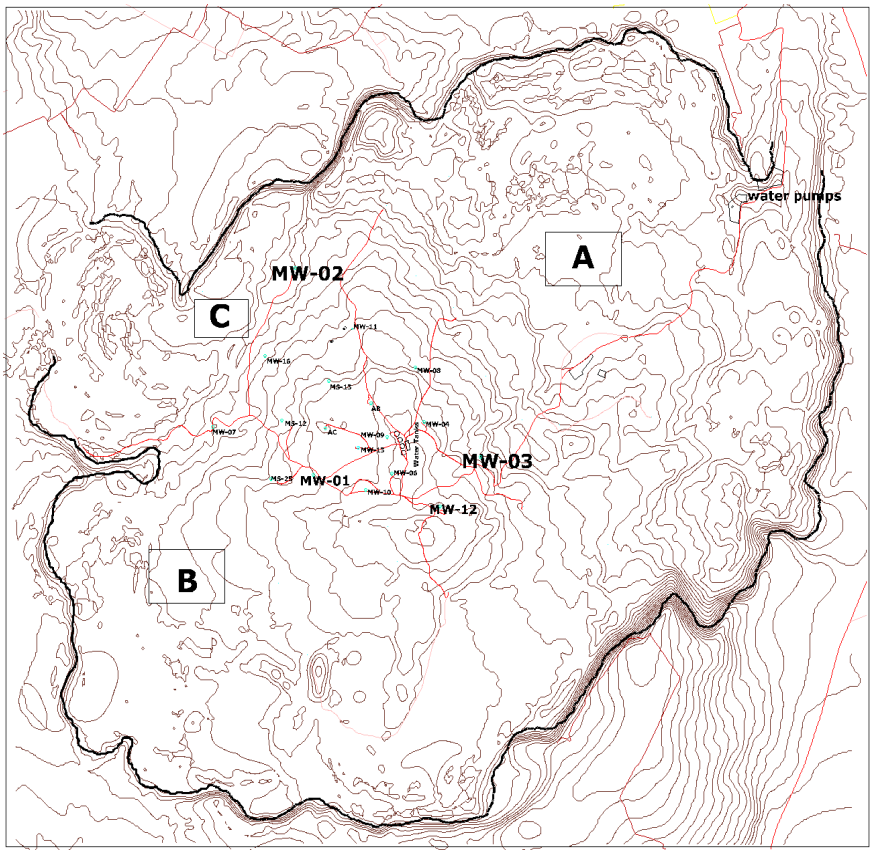

FIGURE 4: A map of Menengai caldera showing possible spa locations, labelled A, B and C

Scenario B:
Under this scenario, the bathing lagoon is located at point B near the caldera rim next to the road exiting into Kabarak, about 1.5 km away from Well MW-01. This location provides a relatively good view of the crater and the caldera. The location has lava outcrops on the surface, creating a more serene and natural atmosphere. This location has about 3000–4000 m^2 of relatively flat surface area available.

Scenario C:
The bathing lagoon is located at point C, about 1 km away from Well MW-02. Since the assumed re-injection point is at Well MW-02 then there is no requirement for a brine supply pipeline, should the spa get its supply from the separated brine. A provision for tee-off along the brine pipeline is sufficient. However in this design, a supply pipeline route is considered from Well MW-03.

An area of 7000 m^2 is proposed for the spa, including the changing rooms, shopping space, restaurantand parking area.

The X and Y co-ordinates indicated in Table 2 are generated from an AutoCAD map used in the distance transform method to calculate the pipe length and the best possible pipeline route.

2.3.4 Spa size and layout

The pipelines, both for supply and re-injection, were designed and an optimum pipe diameter obtained. The geothermal fluid is first delivered into a cooling pond and then into the bathing pond before it is pumped to the cold re-injection point. A stainless steel heat exchanger coil is installed in the cooling pond. This offers two advantages: it will aid in cooling the pond as well as in heating up fresh cold water to be used in the steam room, showers and at the waterfall.

A surface area of water of 2800 m^2 is considered in this design to accommodate 1000 bathers, allowing each bather 2.8 m^2 of water surface area. The average depth of the deepest section is 1.5 m while the shallow section is 0.5 m, hence an average depth of 1 m. The brine exits the pond at approximately 33°C.

TABLE 2: Coordinates of the proposed locations and elevations (see Appendix I)

	Coordinates		Elevations
	X	Y	(m)
Scenario A	8509	9728	1820
Scenario B	3082	5626	2000
Scenario C	3805	9010	1940
MW-02 (proposed for re-injection)	4630	9493	1900
MW-03	7096	7062	1940

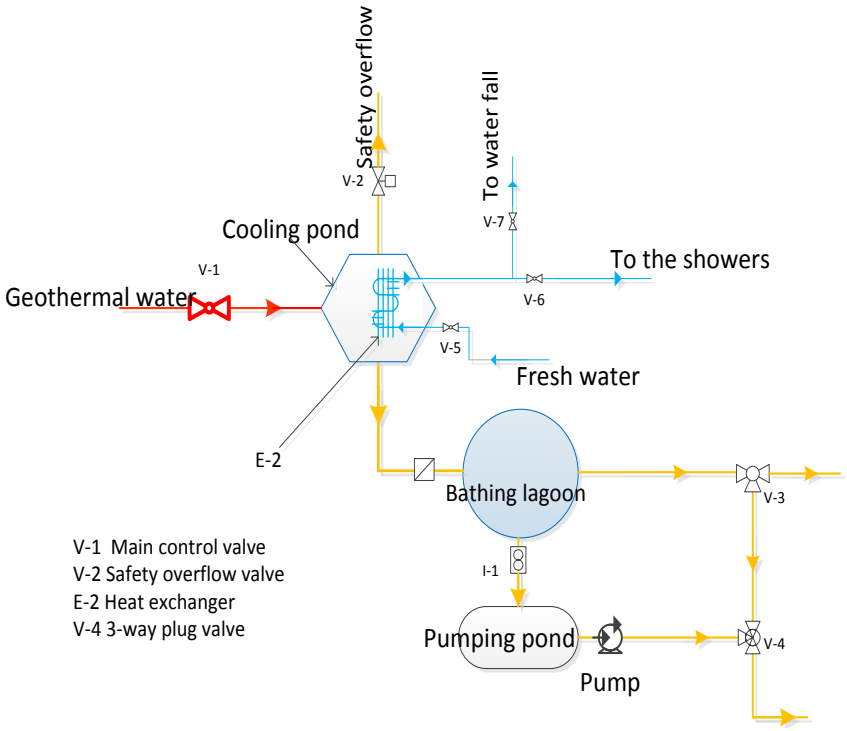

FIGURE 5: Proposed design layout of the geothermal spa

The cooling pond shall be 16 m in diameter and 2 m deep. The layout is as shown in Figure 5.

2.3.5 Pipeline design

Pipe diameter optimization, based on minimum cost, topology and route selection was considered. Route selection was done using the distance transform method. An upward flow of up to 30% was allowed for a pipe route going uphill. Heat losses were calculated assuming an insulation thickness of 0.05 m rock wool and a pipe setup as shown in Figure 6. The summary of monthly weather data for Nakuru used in this report is indicated in Table 3.

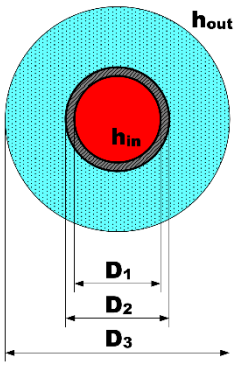

FIGURE 6: An insulated pipe

TABLE 3: Summary of monthly weather data for Nakuru (Source: RETScreen, 2011)

Month	Air Temp. °C	Relative Humidity %	Wind Speed m/s
Jan	18.45	57.6	3.809
Feb	19.2	51.9	3.792
Mar	19.95	56.9	3.965
Apr	18.75	71.4	2.37
May	17.3	74.2	1.811
Jun	17.85	73.4	1.556
Jul	16.8	72.9	1.515
Aug	17.1	72.3	1.616
Sep	17.3	68.6	2.237
Oct	17.5	70.8	1.893
Nov	17.2	74.6	3.154
Dec	16.8	65.7	1.926
Average	**17.85**	**67.5**	**2.47**

The total cost of a pipeline is a parameter used for selecting the optimum diameter. Increase in pipe diameter results in an increase in the total capital cost and, at the same time, decreases the pumping cost.

Optimum pipe diameter was obtained from the following cost calculations:

$$C_t = C_c + C_a(1/(1+i)^T)/i \quad (1)$$

where C_t = Total cost;
C_c = Capital cost;
C_a = Annual cost;
i = Interest rate; and
T = Life time.

The capital costs were calculated from:

$$C_c = L_p k_p + n_b k_b + n_c k_c + n_u k_u + n_v k_v + n_d k_d + L_p k_i \quad (2)$$

where L_p = Pipe length (m);
k_p = Cost of pipe (USD/m);
n_b = Number of bends;
k_c = Cost of a bend (USD/bend);
n_c = Number of connections;
k_c = Cost of a connection (USD/connection);
n_u = Number of expansion units;
k_u = Cost of an expansion unit (USD/expansion unit);
n_v = Number of valves;
k_v = Cost of a valve (USD/valve);
n_d = Number of pumps;
k_d = Cost of a pump (USD/pump); and
k_i = Cost of insulation material (USD/m).

Annual cost was calculated from:

$$C_a = k_e O_h P \quad (3)$$

Where O_h = Operating hours in a year;
k_e = Cost of electrical energy (USD/kWh); and
P = Power of the pump (kW).

Pump power was calculated from:

$$P = g\rho H_{tot}\, Q/\eta \quad (4)$$

where g = Acceleration due to gravity (m/s^2);
ρ = Density of the fluid (kg/m^3);
H_{tot} = Total head (m);
Q = Volumetric flow rate (m^3/s); and
η = Pump efficiency.

The total head is given from the sum of pressure drop caused by friction and the static head due to the elevation difference:

$$H_{tot} = \left(H_f + \Delta Z\right) \quad (5)$$

where H_f = Friction head (m); and
ΔZ = Elevation difference between end and start points (m).

The velocity, *v* had to be calculated, in order to determine H_f:

$$v = Q/(\frac{\pi {D_{in}}^2}{4}) \quad (6)$$

where D_{in} = Inner pipe diameter (m).

The equivalent length, taking into account the pressure drop in fittings and valves, was calculated from:

$$L_e = L_p + n_b h_b D_{in} + n_c h_c D_{in} + n_u h_u D_{in} + n_v h_v D_{in} \quad (7)$$

where L_p = Pipe length (m);
h_b = Ratio of equivalent length to pipe diameter for bends;
h_c = Ratio of equivalent length to pipe diameter for connections;
h_u = Ratio of equivalent length to pipe diameter for expansion units; and
h_v = Ratio of equivalent length to pipe diameter for valves.

The Reynolds number was calculated from:

$$Re = \frac{\rho v\, D_{in}}{\mu} \quad (8)$$

where μ = Dynamic viscosity of the fluid (kg/ms).

If $Re \leq 2100$, then

$$f = 64/Re \quad (9)$$

If $Re \geq 5000$, then

$$f = 0.25/(log_{10}\left[\frac{€}{3.7D_{in}} + \frac{5.74}{Re^{0.9}}\right])^2 \quad (10)$$

where f = Friction factor; and
€ = Absolute roughness of the pipe (m).

The friction head was calculated from:

$$H_f = f v^2 L_e/(2gD_{in}) \quad (11)$$

2.3.6 Energy requirements for the spa

The heat transfer from the open pond occurs in the following ways:

- Convection;
- Evaporation;
- Radiation;
- Conduction; and
- Rain.

Heat loss due to convection, Q_c, in W/m^2:

$$Q_c = h_{co}(T_w - T_a) \quad (12)$$

where h_{co} = Heat transfer coefficient (W/m^2°C);
T_w = Water temperature (°C); and
T_a = Air temperature (°C).

From Rimsha-Doncenko equations, h_{co}:

$$h_{co} = K + 1.88V \quad (13)$$

where K = Constant dependent on the temperatures (W/m^2°C); and
V = Wind speed at 2 m height (m/s).

$$K = 3.89 + 0.17(T_w - T_a) \tag{14}$$

Heat loss due to evaporation, Q_e in W/m^2:

$$Q_e = (1.56K + 2.93V)(e_w - e_a) \tag{15}$$

where e_w = Partial pressure of steam at surface (mbar); and
e_a = Partial pressure of steam in air (mbar).

Heat loss due to radiation, Q_r in W/m^2:

$$Q_r = (4.186(\left(13.18 * 10^{-9} {T_a}^4 (0.46 - 0.06 {e_a}^{0.5}) - G_o(1-a)\right)(1 - 0.012N^2) + 13.18 * 10^{-9}({T_w}^4 - {T_a}^4)) \tag{16}$$

where G_o = Sun's radiation in clear weather;
a = Natural reflection of water; and
N = Cloudiness factor (0-8).

For design purposes we consider the case giving highest energy requirements which is when G_o= 0 and N=0.

Heat loss due to *conduction* is calculated by estimating the heat loss through the walls and bottom of the pool. Heat loss due to *rain* is calculated as the amount of energy needed to heat the rain from the ambient temperature to the pool temperature. These losses are expected to be relatively small.

Heat loss from pipes:
An insulated pipe, as shown in Figure 6, was considered. Heat loss per unit length from insulated pipes is given by:

$$Q = \Pi D_3 U * (T_{in} - T_{out}) \tag{17}$$

where D_3 = Outer diameter including insulation (m);
U = Overall heat transfer coefficient based on outside of the insulated pipe (W/m^2°C);
T_{in} = Fluid temperature (°C); and
T_{out} = Outside air temperature (°C).

$$\frac{1}{U} = \left\{\left(\frac{D_3}{D_1 h_{in}}\right) + \left[\frac{D_3 \ln\left(\frac{D_2}{D_1}\right)}{2k_{pipe}}\right] + \left[\frac{D_3 \ln\left(\frac{D_3}{D_2}\right)}{2k_{ins}}\right] + \frac{1}{h_{out}}\right\} \tag{18}$$

where h_{in} = Heat transfer coefficient inside the pipe;
D_1, D_2, D_3 = Diameters as shown in Figure 6 (m);
k_{pipe} = Thermal conductivity of the pipe material (W/m°C);
k_{ins} = Thermal conductivity of the insulation material (W/m°C); and
h_{out} = Heat transfer coefficient outside the pipe (W/m^2°C).

2.4 Results of pipeline design

A pipeline from MW-03, which is a liquid dominated well (GDC, 2013), was designed to the proposed spa locations in the three scenarios. The supply pipeline is insulated while the re-injection pipeline from the pumping pond is not. In this report, the cost of pumping to a distance of 1 km to a high point from

Well MW-03, requiring one pumping unit at 60 kg/s, was estimated and used to obtain the optimum diameter at the minimum cost for the supply pipeline which was found to be 200 mm (Figure 7).

Temperature drop, with and without insulation of the supply pipeline in scenario C, the longest pipeline in the three scenarios, was calculated using Equations 17 and 18. This was found to be over 17°C without insulation and 2°C with 50 mm thick insulation, for the 4600 m as shown in Figure 8; therefore, there is a need for insulation.

Using the X and Y co-ordinates from Table 2, the distance transform algorithm was used to obtain the shortest appropriate pipeline route (Appendix I) and the pipeline cost was determined.

Table 4 shows the results of the pipeline cost analysis for the three scenarios. Scenario C has the lowest cost because of its location near the assumed re-injection point, hence a shorter pipeline needed for re-injection. A comparison of the supply, re-injection and the total pipeline costs for the three scenarios is shown in Figure 9. Scenario B has the highest total pipeline cost. Scenario A is 12% cheaper than B while scenario C is 32% cheaper than scenario B.

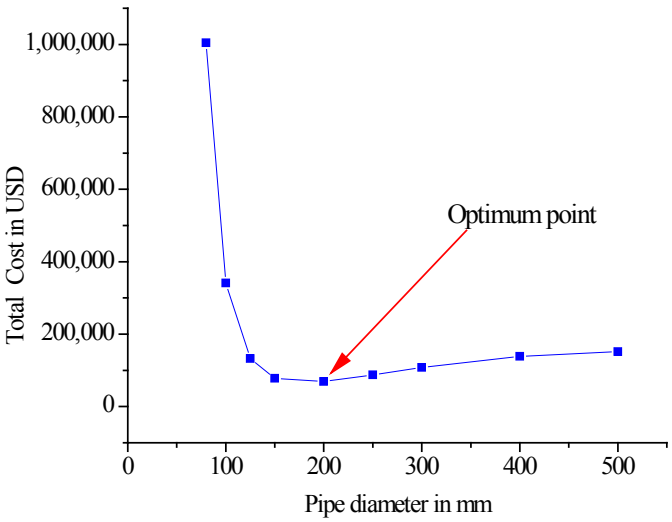

FIGURE 7: Optimum diameter selection based on minimum cost

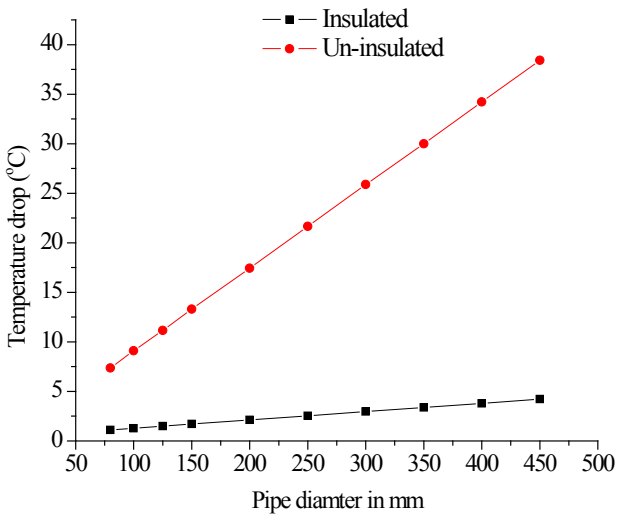

FIGURE 8: Temperature drop in insulated and un-insulated pipes of different diameter

TABLE 4: Pipeline length, diameter and capital cost for the three scenarios

	Supply pipeline ***(Insulated)***			**Re-injection** ***(Un-insulated)***			**Total cost (USD)**
	Length (m)	**Pipe diameter (m)**	**Cost (USD)**	**Length (m)**	**Pipe diameter (m)**	**Cost (USD)**	
Scenario A	3000	0.2	210,000	4700	0.2	290,000	500,000
Scenario B	4500	0.2	305,000	4200	0.2	260,000	565,000
Scenario C	4600	0.2	320,000	1000	0.2	65,000	385,000

Scenario A requires a pump between the spa and the re-injection point. The cost of the pump and pipe supports cost is not included in the pipeline cost analysis shown in Table 4 and Figure 9.

Calculations were done for heat transfer in the cooling and bathing ponds, using Equations 12 to 16, and the results are as shown in Table 5.

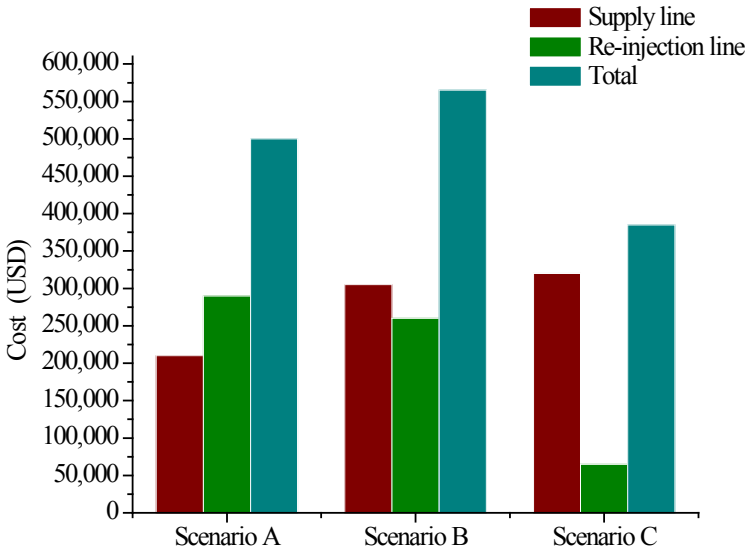

FIGURE 9: Comparisons of pipeline costs for the three scenarios

Geothermal hot water flows into the cooling pond at a 130°C and drops to a 100°C where it is retained for 3 hours. It flows by gravity through a 150 mm diameter pipe at 35 l/s to the bathing pond. Three submersible drainage pumps (Figure 10) are installed in the bathing pond to re-circulate and mix the water, preventing it from forming layers along the depth of the lagoon, with varying temperatures and therefore, assisting in achieving uniform temparatures in the lagoon. The retention time in the main lagoon is found to be 23 hours at 35°C; flow is by gravity into the pumping pond.

TABLE 5: Main geothermal spa parameters

Mass flow bathing pond (kg/s)	Area bathing pond (m^2)	Area cooling pond (m^2)	Retention time bathing pond (hrs)	Retention time cooling pond (hrs)	Temp bathing pond (°C)	Temp geo in (°C)
33.8	2827	201.1	23	2.9	35	130

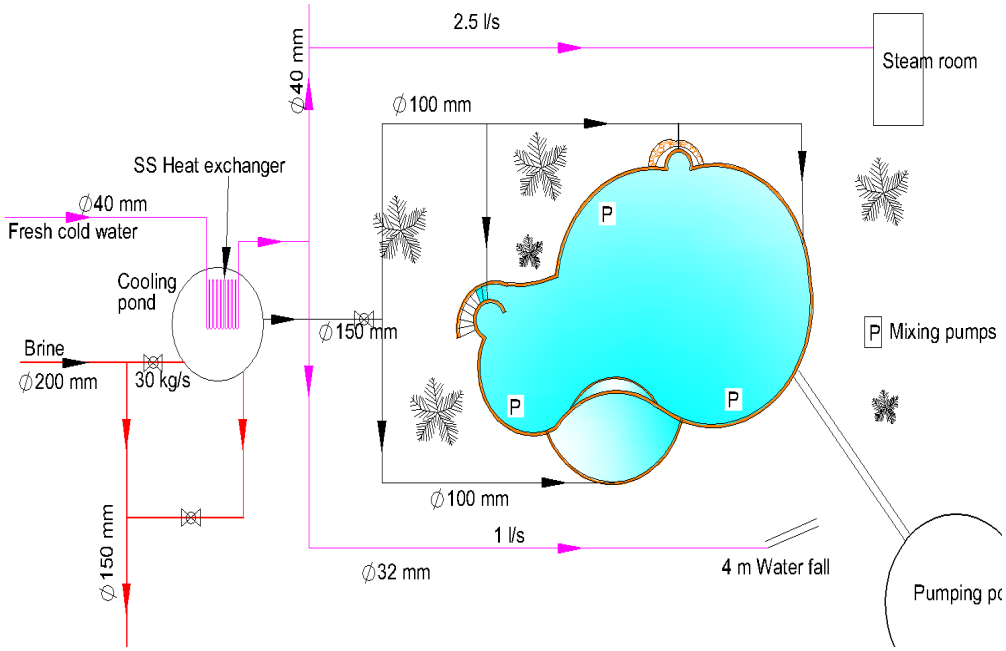

FIGURE 10: Designed spa layout and pipe work

A stainless steel pipe loop, 30 m long and 40 mm in diameter, is installed in the cooling pond as a heat exchanger to heat up cold water from 18°C to 55°C at a flow rate of 8 l/s. This heated fresh water is pumped through the steam jets in the steam room and is also used in the showers before the visitors can take a bath in the lagoon. Scale deposits on the stainless steel loop are expected on the outer side of the pipes and will be cleaned regularly. The piping into the shower is done using high pressure PVC pipes.

A 15 kW pump is used to pressurize the heated fresh water through the steam jets in the steam room. Table 6 shows the designed details of the spa and the steam room.

TABLE 6: Designed details and specifications of the spa

Facility		Parameter	Units	Value
Bathing lagoon		Temperature Retention time Flow rate	°C hours kg/s	35 23 35
Steam room		Dimensions Material	m -	2.1 by 3 by 2 Concrete
	Pumps	Motor rating Flow rate	kW m^3/hr	15 15
	Steam jets	Pressure Flow rates Number	bar l/s -	2 0.6 9
Water fall		Flow rate Dimensions	l/s m	1 4 m high

The retention time in the cooling pond is 3 hours while in the bathing pond it is 23 hours. This allows for aging of the water allowing polymerisation. Various sampling points will be provided in the pipeline between the cooling pond and the bathing lagoon.

3. GEOTHERMAL POOL HEATING

Open-air swimming pools are heated to extend the swimming time or to maintain a temperature that is comfortable to the swimmer. Heating of swimming pools by solar energy has existed for many decades with the technology now well established (Ruiz and Martinez, 2009). However, solar heating is limited due to its intermittence and its un-availability at night. The collectors have to be exposed to the sun, thus requiring relatively large installation areas on the surface, which is not appealing to nature. Control of solar heating is also a challenge.

The size of a swimming pool is largely guided by the number of bathers it can support. According to Halldórsson (1975), the space required for each individual is dependent upon pool depth. International standards for training professional swimmers and swimming competitions also give a guide on the minimum size requirements of a pool (Perkins, 1988).

In Iceland the total annual water consumption in geothermal heated swimming pools is estimated to be 6.9 million m^3 which corresponds to an energy use of 1,300 TJ per year. The specific water and energy demand is about 220 m^3 of geothermal water or 40,000 MJ of energy for heating 1 m^2 pool surface area (Orkustofnun, 2013).

3.1 Water re-circulation and cleaning

Re-circulation of the pool water is the only means that ensures it is cleaned of dirt, that pathogenic bacteria are removed, and that an even pH is maintained in the pool. A range of recommended parameters for swimming pools is shown in Table 7. Most pools are fitted with skimmers or have a deck level channel to help skim the top layer of floating debris. By use of hand held nets and strainer baskets, big solid particles can be mechanically removed. Many particles are not removed using this method, so filtration is required. The filter is made of multiple layers of sand that vary in size. When the water flows through the sand, solid particles are filtered out.

Swimming pools need to be chemically treated to maintain pool water balance and hygiene. Chemicals for swimming pools include various kinds of sanitizers and disinfectants which control the growth of bacterial and algae matter in the pool water. The pH is controlled using either an acid or a basic compound. Chlorine is added to control algal and bacterial growth, waterborne illnesses, cloudy water and insufficient sanitation of the water. A balance tank is provided for in all swimming pools to hold the excess water from the pool and provide a pumping point for re-circulating the water, as shown in Figure 11.

TABLE 7: Recommended range of swimming pool water parameters (EUSSA, 2010)

Parameter	Range
Appearance	Clear and free from suspended matter
pH	7.2 – 8.0
Total hardness	50 – 400 mg/l
Total alkalinity	75 – 200 mg/l
Total dissolved solids	Less than 500 mg/l

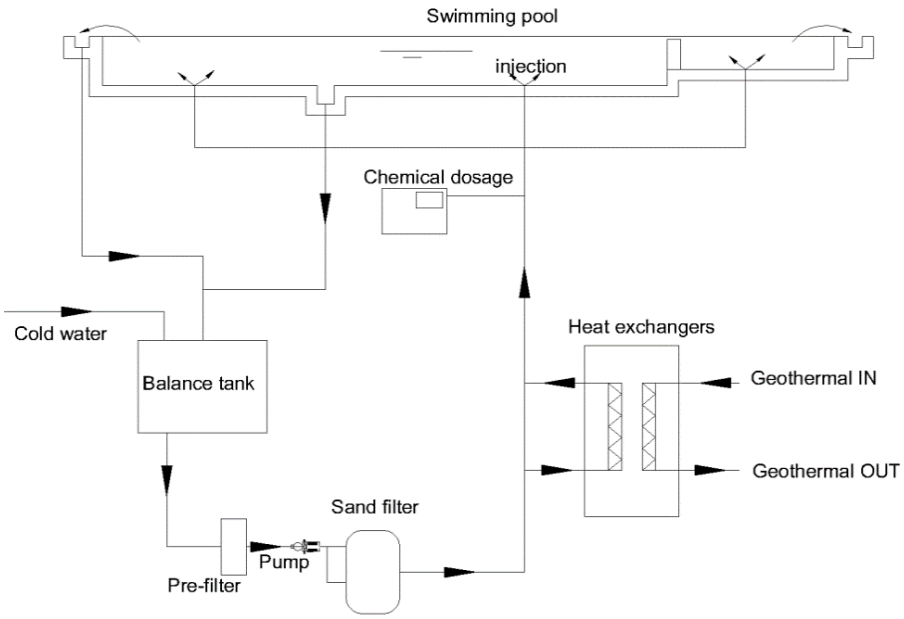

FIGURE 11: Swimming pool circulation layout

The swimming pools considered in this design include a main outdoor swimming pool, an indoor swimming pool, three hot baths, a wading pool, a steam room, a shallow pool and a waterfall (Figure 12), all heated geothermally. All the water is re-circulated. The physical location of the swimming pools is different from the location of the geothermal spa described earlier. The location is not stated in this report, but a location that could suit these swimming pool facilities is in the geothermal complex headquarters.

The significant heat loss from the swimming pools due to evaporation, conduction, convection and rain is calculated as described in chapter 2.3.6. The calculations are based on monthly average climate conditions, given in Table 3. Figure 13 shows a pie which indicates the highest heat loss from a swimming pool is due to evaporation losses, while loss due to rain is the least.

The turnover of the pool water is 4 hours based on the standards and other parameters shown in Table 7 (Perkins, 1988). Heating a swimming pool is largely dependent on weather conditions and the size of the pool.

The total energy required for heating the swimming pools is dependent largely on the wind speed rather than air temperature. The months of January to March and November require the most heating energy. The least required thermal energy is in the month of July as shown in Figure 14.

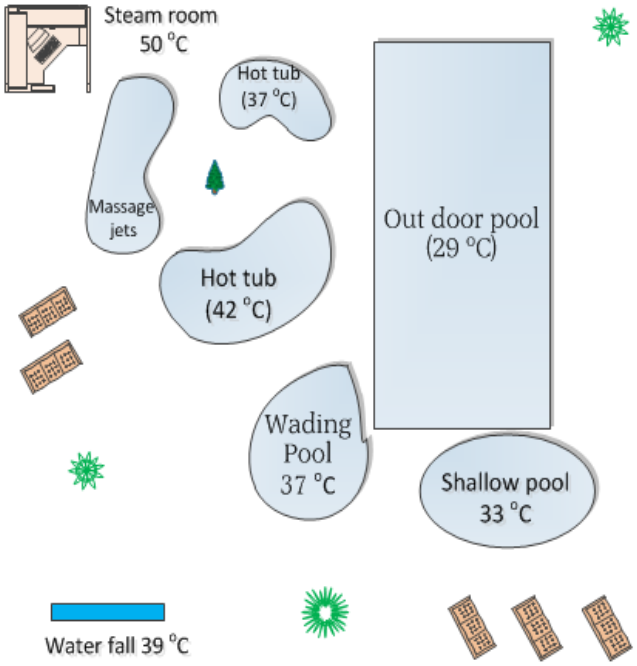

FIGURE 12: Various swimming pools

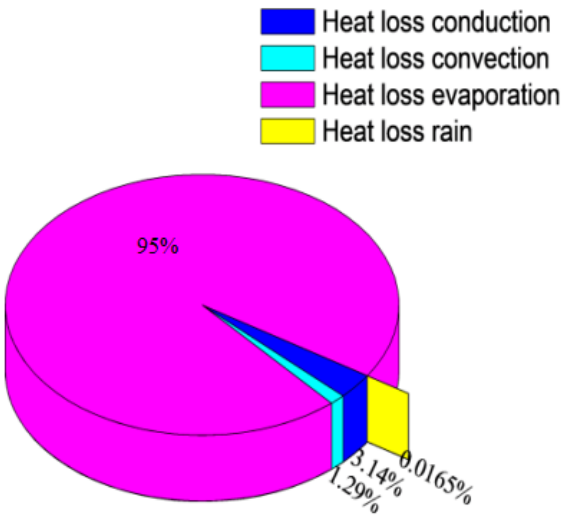

FIGURE 13: Various means of heat loss from the swimming pool

Figure 15 shows the required geothermal flow rates for various designed swimming pools. The geothermal flow rate required for heating the indoor pool water is the least and remains constant throughout the year. This is because the indoor pool is not affected by the outside wind which varies throughout the year. The geothermal flow required for heating the waterfall is constant throughout the year because the water is more exposed than the pool water as it falls down and this exposure factor has more influence than the wind. The outdoor main pool is the most affected by weather variations.

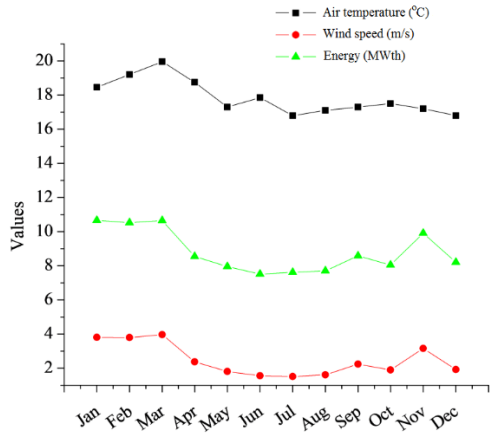

FIGURE 14: Variations of air temperature and wind speed and energy requirements for pool heating in a year

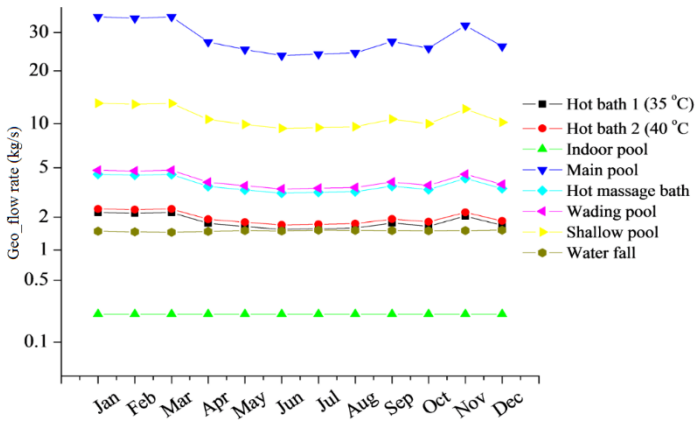

FIGURE 15: Flow rate requirements in the various pools in a year

The average thermal power required to heat all the swimming facilities is 9 MWth. This energy is extracted through heat exchangers from geothermal water at 130°C, exiting at 90°C. The highest thermal power required is 11 MWth between January and March which are the windiest months of the year. The total mass flow required is 55 kg/s.

Table 8 shows the main accessories and equipment for the various swimming pools considered and designed in this report. The turnover mainly depends on the type of facility and its volume.

TABLE 8: Main accessories and equipment for the swimming pool installations

	Main	**Shallow**	**Wading**	**Indoor**	**Hot tub 1**	**Massage tub**	**Hot tub 2**
Area (m^2)	313	113	38	113	18	36	18
Volume (m^3)	469	79	1	101	18	36	18
Turnover (hr)	4.0	4.0	0.2	3.0	1.0	1.0	1.0
Flowrate (m^3/hr)	117	20	5	34	18	36	18
Sand filters	4No CX900	1No CX800	1No CX500	2NoCX800	1No CX800	2No CX800	1No CX800
No. of inlets	17	3	1	5	3	6	3
Vol. balance tank (m^3)	24	4	1	6	1	2	1
Pumps	2No 28kw DE65/20	1No 1.2kw SLL 400	1No 0.6kw DM3	2No 1kw SLL 300	1No 1kw SLL 300	2No 1kw SLL 300	1No 1kw SLL 300
Chlorinator (gms/hr)	79	14	4	23	13	25	13
Type of chlorinator	M4921 1.kw	BMSC20 120w	BMSC20 120w	BMSC26 160w	BMSC20 120w	BMSC26 160w	BMSC20 120w

Table 9 shows the details of the swimming pools. The total combined water surface area of all the swimming facilities is 670 m^2.

TABLE 9: The details of the swimming pool facilities designed

General details: Total land area 4700 m^2 Total water surface area 670 m^2		
Main outdoor pool	L: 25 m W: 12.5 m Area 313 m^2 Volume 469 m^3	Maximum depth 2 m Minimum depth 1 m Temperature 29°C
Indoor pool	L: 15 m W: 7.5 m Area 113 m^2 Volume 101 m^3	Uniform depth 0.9 m Temperature 30°C
Shallow/game pool	Radius: 6 m Area 113 m^2 Volume 79 m^3	Uniform depth 0.7 m Temperature 33°C With a water slide of 51 m track length
Wading pool	Radius: 3.4 m Area 38 m^2 Volume 1 m^3	Uniform depth 0.25 m Temperature 37°C
Hot tubs: 1. 35°C 2. 36°C 3. 40°C	 Radius: 2.4 m, kidney shaped Radius: 3.4 m, kidney shaped Radius: 2.4 m, kidney shaped	Depth of 1 m With 6 massage jets High temperature
Steam room	L: 4 m, W: 3 m	Temperature 55°C 9 steam jets
Waterfall	Height: 4 m, width: 3 m	Temperature 39°C

.

3.2 Heat exchangers

Heat exchangers are usually designed to maximize the surface area that exists between two fluids. Selection of heat exchangers in this design is done by considering the flow rates and temperature differences. Water-water plate heat exchangers are designed for each pool having a separate heating and cleaning system. Table 10 shows the various specifications for heat exchangers for each swimming facility considered in this report

4. COST ANALYSIS OF THE GEOTHERMAL SPA AND CONCLUSIONS

4.1 Cost analysis

The main parameters usually evaluated in an economic analysis include PV (Present Value), NPV (Net Present Value), and IRR (Internal Rate of Return). These are based on two basic adages of finance, according to Breadley et al. (2011) which are "a dollar today is worth more than a dollar tomorrow" and "a risky dollar is worth less than a safe one". In any investment, there is the opportunity cost which is foregone by investing in the project rather than in another one. The rate of return of the foregone project is called the discount rate, *r*.

TABLE 10: Water-water heat exchanger details

Pool type	Side	Temp. in (°C)	Temp. out (°C)	Pressure drop (kPa)	Water volume / Unit (l)	Max. working pressure (bar)	Max. working temp. (°C)	LMTD (K)	Surface area (m^2)
Hot bath 1 (37°C)	A	120	90	4.74	0.063	25	180	78.32	0.13
	B	18	35	9.33	0.084	25	180		
Hot bath 2 (42°C)	A	120	90	6.58	0.063	25	180	75.93	0.13
	B	18	40	8.05	0.084	25	180		
Indoor pool	A	120	90	0.12	0.063	25	180	80.2	0.13
	B	18	31	0.44	0.084	25	180		
Main pool	A	120	90	188.61	0.24	16	180	81.13	0.19
	B	18	29	932.22	0.3	16	180		
Massage tub	A	120	90	16.5	0.063	25	180	77.85	0.13
	B	18	36	30.37	0.084	25	180		
Wading pool	A	120	90	19.68	0.063	25	180	77.37	0.13
	B	18	37	32.75	0.084	25	180		
Shallow pool with slide	A	120	90	125.63	0.063	25	180	79.26	0.13
	B	18	33	313.56	0.084	25	180		
Waterfall	A	120	90	6.58	0.063	25	180	74.96	0.13
	B	18	42	6.83	0.084	25	180		

The Present Value (PV) of a delayed payoff is found by multiplying the payoff (C1) by a discount factor as:

$$PV = Discount\ factor * C_1 \tag{19}$$

The discount factor is expressed as:

$$Discount\ factor = 1/(1+r) \tag{20}$$

To calculate the present value, the expected future payoffs are discounted by the rate of return offered by comparable investment alternatives (i.e. the discount rate). To calculate the Present Value, the cash flows every year (C_1, C_2, C_3,) are discounted by an appropriate discount rate:

$$PV = \frac{C_1}{(1+r_1)} + \frac{C_2}{(1+r_2)^2} + \frac{C_3}{(1+r_3)^3} + \cdots \tag{21}$$

To find the Net Present Value we have:

$$NPV = C_0 + PV \tag{22}$$

where C_0 = Initial investment.

Internal Rate of Return (IRR) is the value of the discounted cash flow (DCF) rate of return that forces the NPV to zero in the period considered. IRR is evaluated by means of iterative calculation from the equation:

$$NPV_{IRR} = C_0 + \sum_{i=1}^{n} \frac{C_i}{(1+IRR)^i} = 0 \quad (23)$$

where n = Number of years considered (project life).

The economic analysis is done for the geothermal spa with an assumed project life of 10 years. In this cost analysis, the following assumptions were made:

- An average price of a ticket for an adult bather is 6 US dollars per visit and increases at 5% per year.
- The spa operates 330 days, paying for 30 days of maintenance in a year.
- The average number of visitors in a year increases by 30%. Visitors in the first year of operation number 25% of the annual number of tourists currently visiting Lake Nakuru National Park.
- The variable and running costs increase at 15% annually.
- The cost of exploration and well drilling is not considered. The price of hot geothermal is assumed to be charged per volume consumed, irrespective of temperature drop. In this report it was assumed as 0.5 USD/m^3. This is a very rough estimation of the price of fresh water in Kenya when sold in bulk for industrial use.
- The discount rate in this report is assumed to be 12%. This is based on the central bank of Kenya Treasury bond coupon rate for a 10 year maturation period, as of August 2013. Treasury bonds are considered as the opportunity cost in this report work.
- This analysis does not consider the main pipeline costs.

The spa project is assumed to generate revenue after one year of initial capital expenditures for construction work. If the start-up year is 2015, then the following financial analysis is done.

The preliminary analysis indicates that the cash flow will be positive after running the project for 2 years (Figure 16). The NPV curve at a 12% discount rate returns a positive value in the year 2019, five years after the assumed project start. This is according to a cumulative present value analysis (Figure 17). With a project life of 10 years, the indication is that the project is viable.

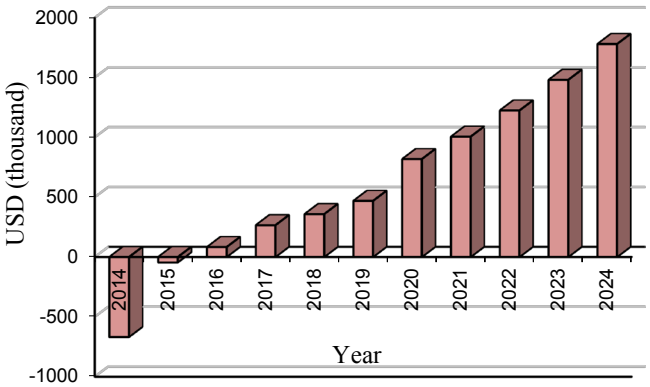

FIGURE 16: Cash flows

According to the analysis, the IRR is 40% for a project life of 10 years. This is higher than the discount rate, indicating the viability of the project. After the 5th year, the IRR analysis indicates a higher rate than the discount rate, as shown in Figure 18.

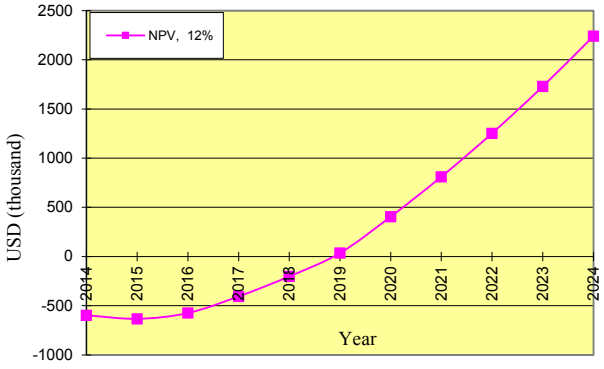

FIGURE 17: Cumulative present values

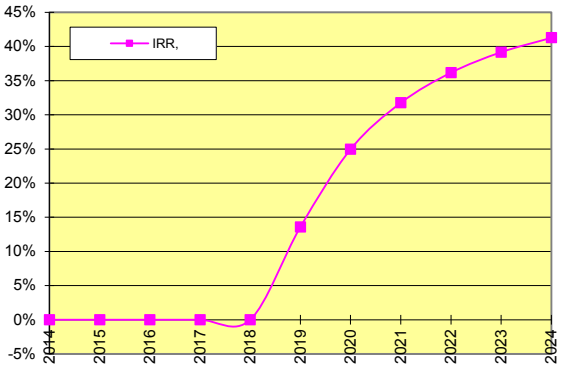

FIGURE 18: Internal rate of return

4.2 Conclusions

A geothermal spa was designed for Menengai geothermal field. There are other factors that may contribute to the site location of the spa other than the pipeline cost alone as considered in this report. Financial gains, leisure as well as utilisation of the available resources which could not otherwise have been utilised, are some of the advantages in the construction of a spa. The nearness of Menengai geothermal field to Lake Nakuru provides an opportunity to attract more visitors as the distance between is relatively short. The fact that Menengai already attracts visitors, students, scholars and other professionals is a key indicator of the potential that exists in the field. This preliminary research work indicates that design and construction of a spa in Menengai is possible and could offer various benefits, among them financial. Health tourism will be greatly promoted whereby the tourists spend their spare time improving their health and wellbeing. With geothermal sites and power plants attracting visitors, scholar and students, this forms a potential for many tourists to visit the health spa. Heating of a conventionally circulated swimming pool was also discussed.

Further research on silica scaling, the financial perspective and additional sources of geothermal water is recommended.

5. GEOTHERMAL CROP DRYING

5.1 Background

Drying is one of the oldest methods of preserving food, and it is fairly simple, safe and can be done all year round if it done indoors under controlled conditions. It entails the removal of moisture from the product. Each type of crop has its own drying requirements. Some of the crops which require drying are cereals, tea, vegetables and fruits which are extensively grown in Kenya and are dried to a moisture content of below 13%. In addition to crops, fish and meat products also require drying for preservation purposes.

Maize is the largest cereal grain grown in the Rift Valley regions and is sun dried on a small scale, while on a large scale, diesel power is used at government or privately owned grain drying and storage facilities. Maize has continued to be the most important food crop in Kenya, playing an integral role in national food security. Kenya produces around 3 million tonnes of maize per year (Figure 19); about 15% is sold directly to the National Cereals and Produce Board and large millers. The total area under maize cultivation as of the end of 2003 stood at 1.6 million hectares (KNBS). Maize growing in Kenya is concentrated in the Rift Valley districts of Trans Nzoia, UasinGishu and Nakuru (Figure 20). The region is often referred to as the 'Granary of Kenya' (EPZA, 2005).

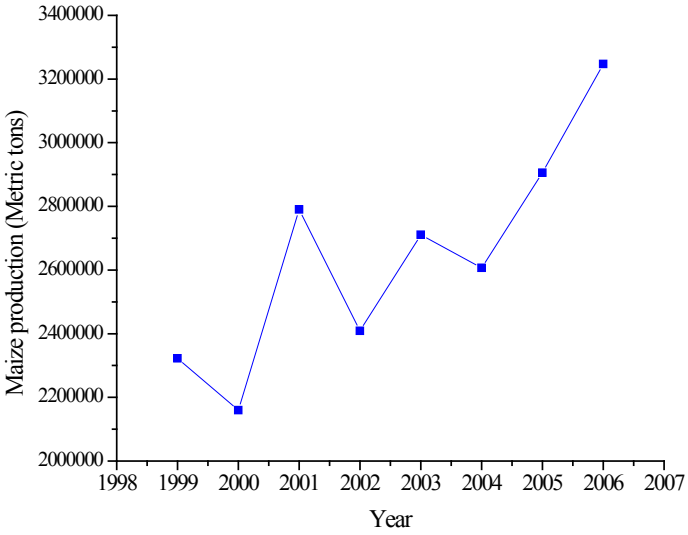

FIGURE 19: Maize production in Kenya (KNBS, 2012)

Tea and coffee are dehydrated as part of their manufacturing process. This is done at the processing factories. Vegetables are dehydrated to enhance their storage, minimise losses and enhance their availability during dry weather spells.

The Ministry of Agriculture has the overall responsibility of the grains sector, with the National Cereals and Produce Board, established in 1985 to regulate and offer drying, marketing and storage services in the sector.

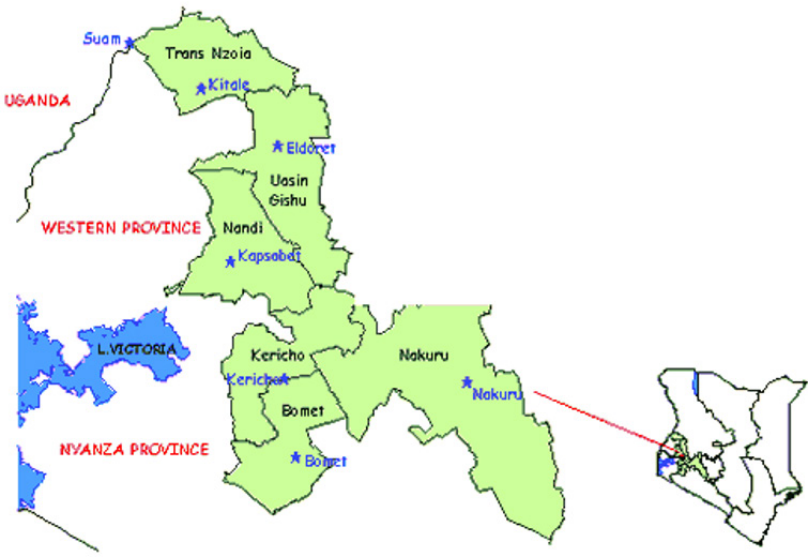

FIGURE 20: Map of Kenya showing grain growing areas (MOA, 2001)

5.2 Crop drying in Kenya

5.2.1 Sun drying

Maize dries partially on the farms through solar drying. For storage purposes, further drying is required to reduce the moisture content from 27% to a 13% dry basis. The small scale farmers achieve this through sun drying for relatively many days (5 to 45 days), where maize is dried on the ground on spread canvas (Figure 21). This is done along the roadsides or in open fields. Dust, laden with fungal spores, can easily be deposited on the maize. Furthermore, sun drying is weather dependent, unreliable and impractical for large volumes of maize. In this case, commercial dryers are utilised.

5.2.2 Geothermal drying

A pyrethrum crop dryer, which utilizes geothermal heat, exists at Eburru, near Naivasha. The steam from a shallow well is piped through galvanized iron pipes and is used to dry flowers and maize, as shown in Figure 22. The well was drilled in the 1940s and farmers utilized the geothermal energy to dry pyrethrum flowers (Mwangi, 2005).

5.2.3 Fossil fuel use in drying

The National Cereals and Produce Board of Kenya, owned by the government, operates its own dryers and charges for drying and storage of maize, wheat and barley. The dryers are powered by industrial diesel oil heaters. Use of fossil fuels leaves a negative carbon footprint on the environment. Thus, there exists significant potential to utilize clean geothermal heat for drying operations.

FIGURE 21: Sun drying of grains

FIGURE 22: Pyrethrum drying using geothermal heat in Eburru, Kenya

A privately owned drying firm, Lesiolo Grain Dryers, also based in Nakuru, provides drying services and post-harvest management of grains including wheat, maize, barley and sorghum. It has a combined storage capacity of 80,000 metric tons and 6 dryers of capacities ranging from 10 to 100 tons, all using industrial diesel oil. In addition, it has two mobile dryers of 13 tons capacity each, which are either operated from a tractor PTO or diesel powered with a 200 litre fuel tank capacity, operating in a temperature range of 40 to 60°C.

5.3 Theory of grain drying

The main objective of drying agricultural products is to reduce the moisture content to certain levels that allow safe storage over an extended period of time. It also brings about a reduction in weight and volume, minimizing packaging, storage and transportation costs (Kavak Akpinar et al., 2006). Thermal drying is most commonly used and involves the vaporisation of moisture within the product by the application of heat with subsequent evaporation from the product. Thus, in thermal drying, there is simultaneous heat and mass transfer.

Drying is an energy intensive operation. In most industrialized countries, the energy used in drying accounts for 7–15% of the nation's industrial energy, often with relatively low thermal efficiencies ranging from 25% to 50% (Kavak Akpinar et al., 2006). Agricultural crop drying has been reported to account for about 12 to 20% of the energy consumption in the agricultural sector (Liviu and Badea, 2009).

During the drying process, food materials undergo physical, chemical, and biological changes which can affect some natural attributes like texture, colour, flavour, and nutritional value. Changes in colour and flavour are most important to crops like tea, fruits and vegetables. The drying process influences these factors and, therefore, the quality of the final product. Drying of grains is mainly divided into four broad categories: low-temperature drying using unheated air; medium-temperature drying, below 43°C for seeds and below 60 °C for grains to be milled; high-temperature drying where kernel temperatures are maintained below 82°C for animal feeds; and combination drying using both low and high temperatures (FAO, 2008). The optimum grain drying temperature depends on the dryer type, the grains species and the grain quality requirements.

The importance of a dryer is to supply the product with more heat than is available under ambient conditions, thereby increasing the vapour pressure of the moisture held within the crop and decreasing significantly the relative humidity of the drying air and increasing its moisture carrying capacity, ensuring sufficiently low equilibrium moisture content.

5.3.1 Drying kinetics

Thermal drying involves two simultaneous actions: a heat transfer process by which the moisture content of the solid is reduced and a mass transfer process where there is fluid displacement within the structure of the solid towards its surface and evaporation. The quality and quantity of energy as well as heat and mass transfer should be investigated throughout the drying processes.

5.3.2 Water activity

Water activity (a_w) is the ratio of the vapour pressure of water in a material to the vapour pressure of pure water at the same temperature. The water activity of a sample is equal to the relative humidity of air, when there is equilibrium of vapour pressure and temperature. Water activity is temperature dependent. Temperature changes water activity due to changes in water binding, dissociation of water, solubility of solutes in water, or the state of the matrix.

$$a_w = \frac{p}{p_o} \tag{24}$$

where p = Vapour pressure of water in the product; and
p_o = Vapour pressure of pure water at the same temperature.

Water activity affects the shelf life, safety, texture, flavour, and smell of foods and it is the most important factor in controlling spoilage.

5.3.3 Moisture content

Moisture content of a substance is expressed as a percentage by weight on a wet or dry basis. The moisture content is presented as relative to dry basis, because the dry basis concept is the common basis in the drying research area. A commonly used simple model, assuming that the resistance for water transport is all over the surface of the particle, is represented by an equation analogous to Newton's law of cooling, the Lewis equation (Lewis, 1921):

$$\frac{dM}{d\theta} = -k(M - M_{eq}) \tag{25}$$

where M = Moisture content;
M_{eq} = Equilibrium moisture content;
θ = Time; and
k = Drying constant dependent on the product.

The moisture content attained by a product with respect to a set of atmospheric temperatures and relative humidity is called the equilibrium moisture content. In such conditions, the grain moisture is in equilibrium with the surrounding air. Moisture storage requirements for some grains is shown in Table 11.

TABLE 11: Moisture requirement for storage of grains

Crop	Moisture content for storage (% w.b)	
	For one year storage	For two year storage
Maize	13	11
Wheat	13-14	11-12
Barley	13	11

According to Henderson and Pabis (1961):

$$\frac{M_{final} - M_{eq}}{M_{initial} - M_{eq}} = e^{-k\theta} \tag{26}$$

where $M_{initial}$ = Initial moisture content; and
M_{final} = Final moisture content.

5.4 Grain dryers

Grain dryers can either be unheated air dryers or heated air dryers:

Unheated or natural air-drying is usually performed in a storage bin for a relatively small volume of grain. The period of drying is very much dependent on the weather and could take relatively long to completely dry. Turning of grains is usually performed to ensure uniform and continuous drying.

Heated air dryers can be deep bed dryers or thin layer dryers. In deep bed drying, the condition of the drying air at any point in the grain mass changes with time and the depth of the grain bed. The rate of drying is slower when compared to thin layer drying of grain. The heat should not be more or less than the required amount for evaporation to avoid hardening, discolouration or other unsuitable outcomes (Tesha, 2006).

The most common shapes in deep bed drying are round or rectangular. For efficient operation of deep bed dryers, the air flow rate of 2.94 - 3.92 m³/minute per tonne is recommended. An air flow rate that

is above 3.92 m³/minute per tonne may result in uneven drying and is expensive in operation. If the moisture content of grains is up to 18%, the layer depth of grain should be limited to 3 m and, above 18%, the moisture depth recommended is 2.5 m. The net perforated area of the floor should be 15% of the total floor area. An air velocity of 300 m/minute through opening is preferable.

Thin layer drying refers to the grain drying process in which all grains are fully exposed to the drying air under constant drying conditions. Most commercial dryers are designed on thin layer drying principles. In this case, two periods of drying are usually encountered: the constant drying rate where the rate of evaporation under any given set of air condition is independent of the solid and is essentially the same as the rate of evaporation from a free liquid surface under the same conditions; the falling rate period enters after the constant drying rate period and corresponds to the drying cycle where the product surface is no longer wet and continually decreases until the surface is dry.

5.5 Factors influencing the quality of dried product

Several factors affect the quality of dried product. These include quality of raw material, drying rate and drying temperature.

5.5.1 Raw material quality

Agricultural materials can be either hygroscopic (absorbing moisture from the air) or non-hygroscopic. The quality of the dried product can only be as good as the material from which it was derived. Food products like fish and meat products are usually sensitive and heavily dependent on the raw material quality. Fruit products can be sliced to obtain better and more evenly dried products.

5.5.2 Drying rate

A very fast drying rate can cause shrinkage while a slow rate could result in loss rehydration capacity or increase costs. The drying rate is dependent upon several factors, namely air temperature, air flow rate, relative humidity, exposure time, variety and size of grain, initial moisture content, and grain depth.

The rate of drying increases with the rise of air temperature. According to Henderson and Pabis (1961) the air rate has no observable effect on thin layer drying of wheat when air flow is turbulent. However, for paddy rice and maize, it has been found that the air rate has an effect on the rate of drying. Increasing air humidity decreases the rate of drying while the increase in exposure time of drying air in a single pass increases the drying rate.

The empirical drying equation for maize is:

$$M_{eq} = 0.01 * \left[\frac{LN(1 - rh_{amb})}{-8.65 \cdot 10^{-5}(T_{amb} + 49.810)}\right]^{\frac{1}{1.8634}} \quad (27)$$

where rh_{amb} = Relative humidity of ambient air; and
T_{amb} = Ambient temperature (°C).

5.5.3 Drying temperature

Different products have an optimum drying temperature. Very high temperatures lead to distortion of the chemical composition or may even result in 'cooking' the product. The optimum temperature for maize drying is 49°C. Tea is dried at a temperature range of 60-100°C, depending on the desired flavour.

A very high drying temperature for fish can also lead to case hardening, which may be prevented by controlling the relative humidity and temperature of the drying air (Sotocinal, 1992).

5.6 Mass and heat balances

The rate of air flow required for drying may be calculated by making a heat balance. The heated air drying system is represented in Figure 23.

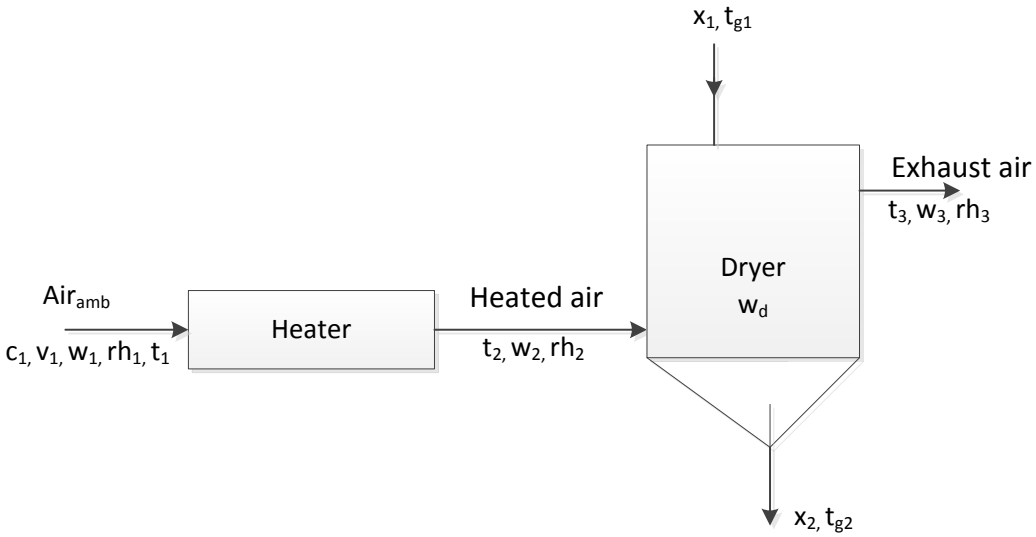

FIGURE 23: Heated air drying system

where c_1 = Air flow rate (m^3/hr);
w_1, w_2, w_3 = Humidity ratios of ambient, heated and exhaust air, respectively (kg/kg);
rh_1, rh_2, rh_3 = Relative humidity of ambient, heated and exhaust air, respectively;
t_1, t_2, t_3 = Temperature of ambient, heated and exhaust air, respectively;
w_d = Weight of bone dry grain in the dryer (kg);
x_1, x_2 = Initial and final moisture contents of grain (kg/kg);
t_{g1}, t_{g2} = Initial and final grain temperatures (°C); and
v_1 = Specific volume of air (m^3/kg).

Heat supplied by drying air, q_a is given by:

$$q_a = \big((0.24 + 0.45w_1) * G_o(t_3 - t_2)\theta\big) * 4.187 \quad (28)$$

where q_a = Heat supplied by air (kJ);
θ = Drying time (hours); and
G_0 = Rate of air supply (kg/hr).

Heat required for evaporation of moisture from the grain, q_1 is given by:

$$q_1 = w_d(x_1 - x_2)\lambda \quad (29)$$

where q_1 = Heat required for operation (kJ); and
λ = Average value of latent heat of vaporisation of moisture from the grain (kJ/kg).

Sensible heat required to raise the grain temperature is given by:

$$q_0 = w_d c_g\big(t_{g2} - t_{g1}\big) + w_d c_w\big(t_{g2} - t_{g1}\big)x_1 \quad (30)$$

where q_0 = Sensible heat required to raise the temperature of the grain and its moisture (kJ); and
c_g, c_w = Specific heats of grain and water, respectively (kJ/kg°C).

The overall mass and energy balances in a drying system give information on dryer performance and parameters of dryer design.

Using energy and mass balance:

$$q_a = q_1 + q_0 \tag{31}$$

And solving for G_o:

$$G_o = \frac{W_d[(x_1 - x_2)\lambda + c_g(t_{g2} - t_{g1}) + c_w(t_{g2} - t_{g1})x_1]}{((0.24 + 0.45w_1) * (t_3 - t_2)\theta) * 4.187} \tag{32}$$

and

$$G = G_o * v_1 \tag{33}$$

where v_1 = Specific volume of humid air (m^3/kg).

Fuel consumption rate:

$$rate_{diesel} = \frac{q_a}{\eta * \eta_b * \eta_{ex} * C_n} \tag{34}$$

where $rate_{diesel}$ = Fuel rate (kg/hr);
C_n = Calorific value of fuel (kJ/kg);
η = Efficiency of the heating system;
η_b = Efficiency of boiler; and
η_{ex} = Efficiency of the heat exchanger.

Design of fan and blowers
Selection and design of a centrifugal blower is done for a given airflow rate and static pressure. Specific speed (N_s) for the specific static pressure, air flow rate and designed motor speed are found by:

$$N_s = \frac{N\sqrt{Q}}{P_s^{0.75}} \tag{35}$$

where N = Speed of the motor (rpm);
Q = Air flow rate (cubic feet/min); and
P_s = Static pressure (inches of water).

The type of air moving unit which would operate at high efficiency is determined at or near peak efficiency at the calculated specific speed, from fan efficiency curves (Appendix II). If more than one type of air moving unit has good efficiency, a final selection can be based on other factors such as relative cost, size and shape of space available and the characteristics of the air flow path (Shirbhate, 2013).

The typical value of the pressure coefficient, Ψ, is found by interpolation, for the type of fan or blower selected and the value of specific speed, N_S. The impeller diameter is found from:

$$\Psi = \frac{2.35 \cdot 10^8 P_s}{N^2 d^2} \tag{36}$$

where ψ = Pressure coefficient; and
d = Diameter of the impellor (inches).

The typical value of the flow coefficient is found from the fan characteristics table and the width is calculated as follows:

$$W = \frac{175Q}{\Phi N d^2} \tag{37}$$

where W = Width of the impellor (inches); and
Φ = Flow coefficient.

Geothermal heating requirement
The heat supplied by air is equivalent to the heat energy from geothermal. The total amount of geothermal supplied, Geo_{amount} is given by:

$$Geo_{amount} = q_a * (T_{in} - T_{out}) * c_w \quad (38)$$

where Geo_{amount} = Total amount of geothermal utilised (kg);
T_{in} = Entry temperature of geothermal in the heat exchanger; and
T_{out} = Exit temperature of geothermal in the heat exchanger.

The geothermal flow rate, $\dot{m}$ in kg/s is given by:

$$\dot{m} = \left(\frac{Geo_{amount}}{3600 * \theta}\right) \quad (39)$$

For diesel use, the total cost of diesel fuel in USD is given by:

$$Cost_{diesel} = rate_{diesel} * \theta * price_{diesel} \quad (40)$$

where $price_{diesel}$ = Price of diesel (USD/l).

The cost of geothermal in USD is calculated from:

$$Cost_{geo} = Geo_{amount} * price_{geo} \quad (41)$$

where $price_{geo}$ = Price of geothermal (USD/kg).

5.7 Design of a geothermal crop dryer

5.7.1 Type, size and shape

The design of a heated grain dryer varies with the method of drying, whether a static deep bed batch dryer or the continuous flow batch dryers (mixing or non-mixing type). A static batch dryer is designed in this research work. The components include the drying chamber, air distribution system, indirect air heating system and the blower. The capacity of the dryer is 20 tons of maize at ambient air conditions. The tunnel/bed type of the dryer is adopted in this design in order to accommodate a wide variety of agricultural products, with minimal modification to the air flow duct and temperature regulation. The thickness of the grain layer exposed is limited to the depth of each tray and fixed to 10 cm. The dryer shall be a tunnel type where the air is blown from the side of the drying chamber and flows along the trays. This is appropriate when drying high moisture products and air re-circulation is necessary. When the air direction is vertical from below, then it is a bed dryer and the choice depends on the type of crop being dried. This also allows for comparing the efficiency of the heat exchanger for both air flow types. An air diversion valve is provided for changing the air flow from tunnel to the bottom of the drying trays.

5.7.2 Drying tea, fruits and vegetables

The processing steps in manufacturing black tea are plucking, withering, maceration, fermentation and drying. Withering reduces the moisture content to about 70% wet basis. It is then dried for about 1 or 2 hours depending on the desired flavour, at a temperature range of 70 to 120°C to a moisture content of 3% (Temple et al., 2000). According to Panchariya et al. (2002), the air velocity is considered to be 0.25 to 0.65 m/s or less.

Fruits and vegetables are considered shrinkable products after drying. The drying kinetics used in this design are based on experimental work by Kowalski and Mierzwa (2013), with an air temperature of 50°C and air flow velocity of up to 1.2 m/s. These parameters for drying tea and vegetables are used to predict the energy requirements by using the model of the designed tunnel dryer.

5.7.3 Air recirculation

The drying temperature depends upon the characteristics of the products. The air can be circulated with the help of a fan and blown in counter-current direction to the flow of the solid (Maharjan, 1995). If the temperatures are too high, the food products may cook or may cause case hardening where moisture is trapped inside the product. On the other hand, too low drying temperatures slow down the drying time and may lead to spoilage of moisture sensitive products like fish and meat products. During the initial drying stages, the moisture evaporates quickly from the product. When the surface moisture is lost, the outside begins to feel dry and the rate of evaporation slows down as the product warms up. It becomes important to recirculate the relatively humid air and prevent case hardening. In drying at a temperature of 49°C and air exiting at 43°C, we have the air properties during the drying process shown in Appendix III. The ambient air is 19°C with 67% relative humidity. The recirculated air properties are as shown in the process labelled "B" in Appendix III at 49°C and 42% relative humidity. This will require 25% fresh ambient air resulting in energy saving while maintaining the product. The designed pilot dryer for drying maize is shown in Figure 24 and the details for the trays are shown in Figure 25.

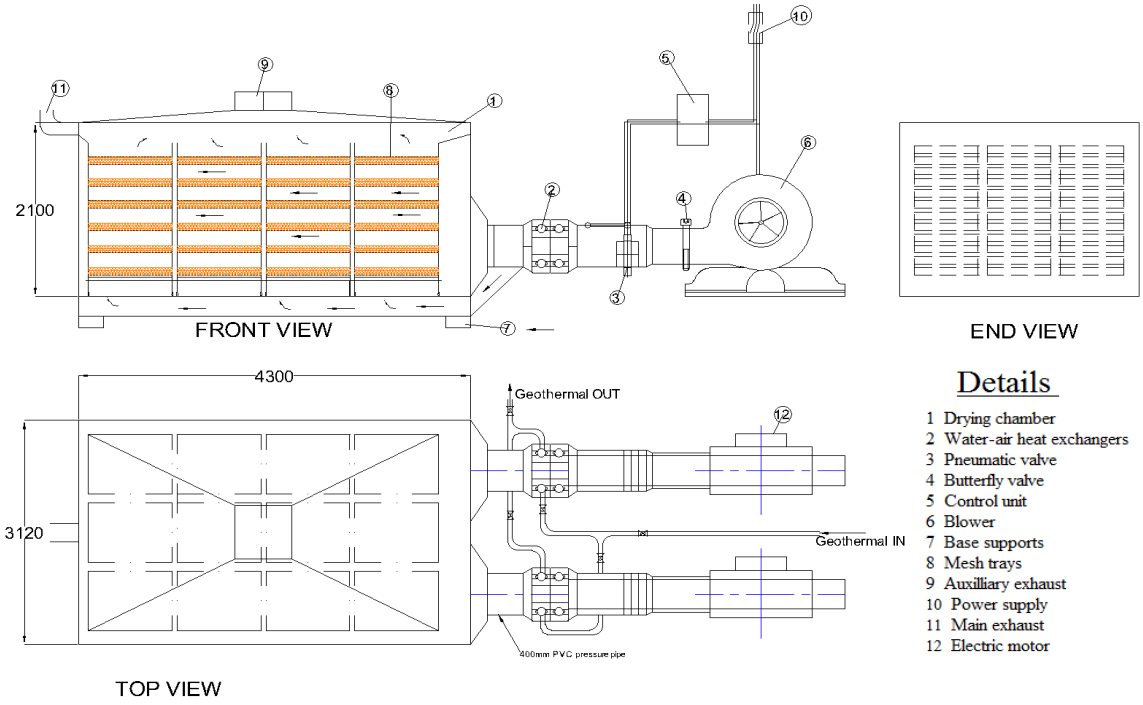

FIGURE 24: Designed crop dryer

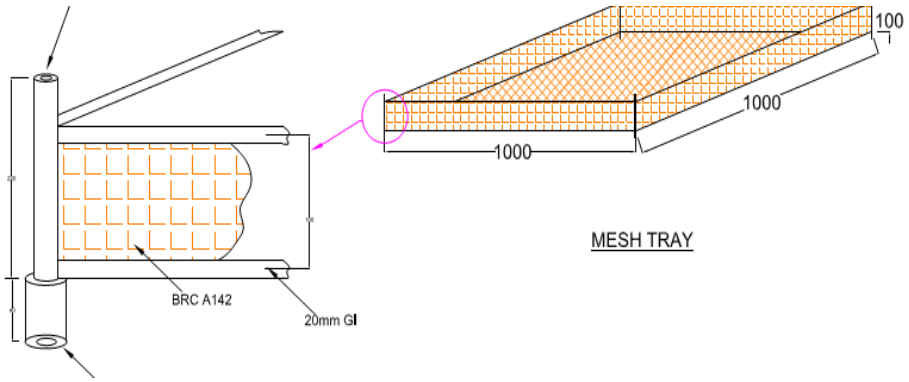

FIGURE 25: Details of the designed drying trays

In drying maize, air is blown into the heat exchanger at an ambient temperature of 19°C and heated to 65°C, and exits the drying chamber at 49°C. Control of geothermal flow into the water-air heat exchanger is then necessary, depending on the product being dried.

The design model was run for different maize capacities and different drying hours to determine the variations in the required flow rate as shown in Figures 26 and 27.

Figure 26 shows the variation of geothermal flow rate for different drying times for maize grains. Drying time is dictated by the amount of moisture to be removed and the type of product. For a higher volume of products, it is recommended to use a longer drying time when using relatively small pipe diameters or when the geothermal mass flow is not sufficient. The geothermal flow rate decreases exponentially with an increase in drying time as shown in Figure 27. The amount of heat energy required for various weights of maize is shown in Figure 28.

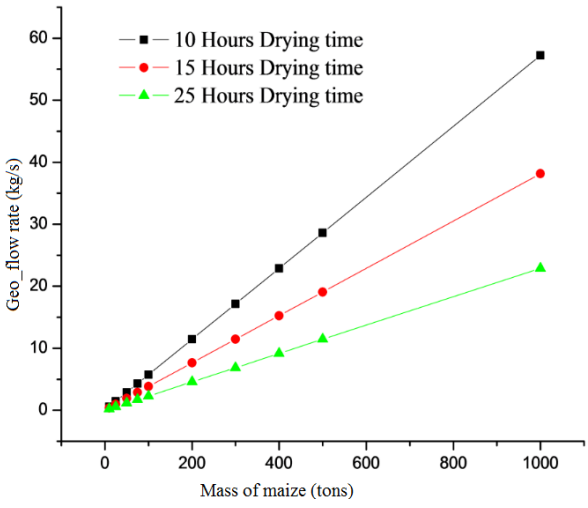

FIGURE 26: Variation of mass flow for different masses of maize

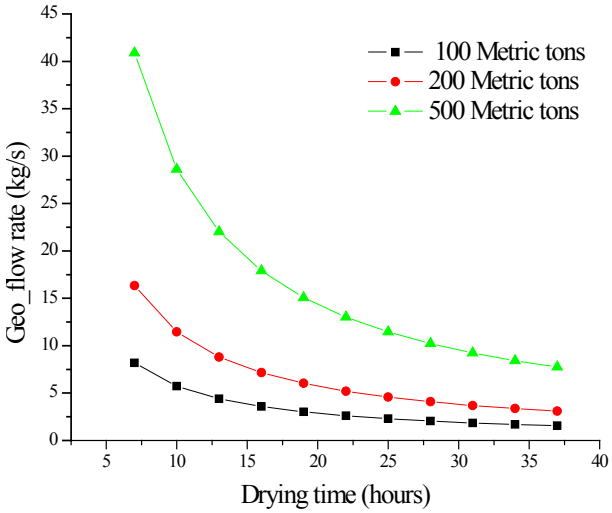

FIGURE 27: Mass flow against time for various grain capacities

Both the rates of geothermal usage and diesel usage increase lineally with an increase in the mass of grains being dried as shown in Figure 29.

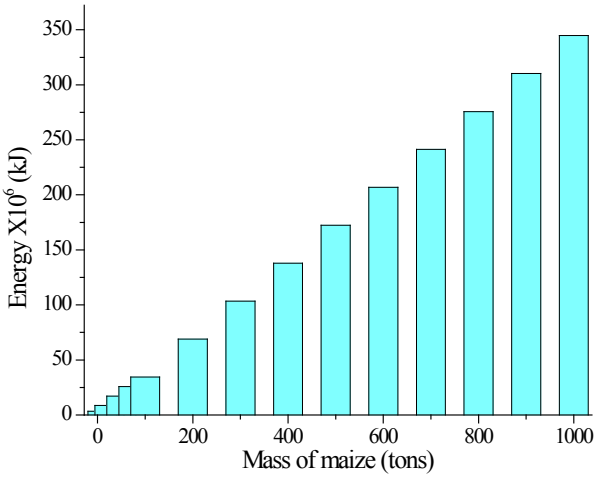

FIGURE 28: Heat energy requirement for various masses of grains

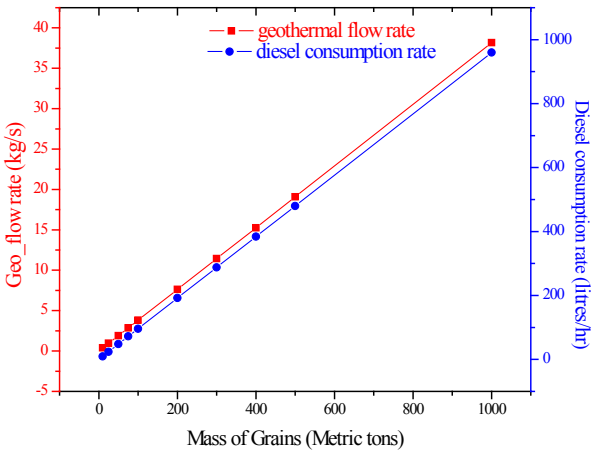

FIGURE 29: Geothermal flow rate and diesel consumption rates for drying different masses of grains

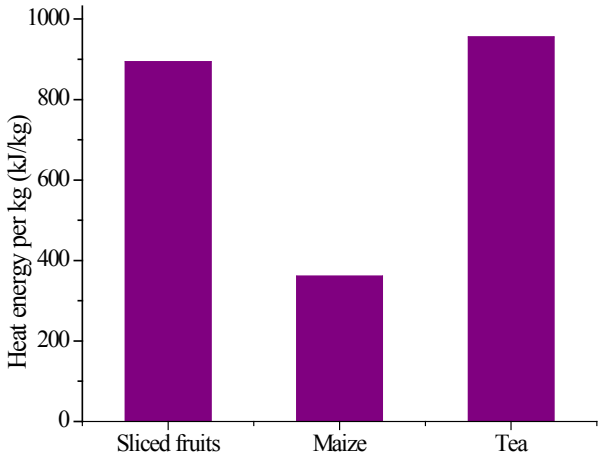

FIGURE 30: Heat energy per kg for drying different crops

The dryer can be used to dry other agricultural products. A test on drying tea and vegetables (tomatoes) was done in the design model and is shown in Figure 30. The energy per kilo of dried product for sliced tomatoes and tea is higher than that of maize, mainly because of higher moisture content in these products. The design parameters are summarised in Table 12.

TABLE 12: Designed dryer inputs and calculated outputs

Inputs			
	Parameter	**Units**	**Value**
Grain	Initial moisture content (db)	%	27
	Final moisture content (db)	%	13
	Grain drying temperature	°C	49
	Grain density	kg/m^3	721
Dryer	Volume	m^3	30
	Type : Tunnel/tray	-	-
Air	Ambient temperature	°C	19
	Relative humidity	-	0.68
	Atmospheric pressure	kPa	88
Geothermal	Entry temperature	°C	130
	Exit temperature	°C	93
	Flow rate	kg/s	2
Calculations			
Dryer	Mass of grain dried	tonnes	15
	Evaporated moisture	tonnes	2
	Thermal energy	kWt	250
	Drying time	hours	7
	Quantity of geothermal used	tonnes	40
	Air velocity	m/s	0.5
	Static pressure	mm H_2O	300
Heat exchanger (water-air)	Max. operating pressure	bars	24
	Number of fins	-	12
Centrifugal blower	Air flow rate	cubic ft/min	14000
	Static pressure	mm H_2O	400
	Motor rating	HP	30
	Operating temperature	°C	150

6. CONCLUSIONS

A geothermal crop dryer was designed and the energy required to dry grains was evaluated. The same dryer can be used for drying more crop varieties and can be experimented upon. Air re-circulation is a means of saving energy and maintaining high drying quality and can be implemented as indicated in this report.

The recommendation from this work, is to evaluate the drying efficiency of this dryer against drying various crops and do a cost comparison with diesel. The quality of the dried crops with regard to nutrients and shrinkage properties should be analysed and reported. Cascaded application with drying should be studied further among other applications.

ACKNOWLEDGEMENTS

I would like to thank my employer, Geothermal Development Company, for granting me the opportunity to attend this training programme. I am also grateful to the former director, Dr. Ingvar B. Fridleifsson and the current director Mr. Lúdvík S. Georgsson, for the successful organization of the programme. Many thanks go to my supervisors, Dr. Árni Ragnarsson and Prof. Sigurjón Arason for their good guidance, for sharing their knowledge and for supervision of this work. My thanks also go to Mr. Jóhann F. Kristjánsson for his assistance. Sincere thanks to Ms. Thórhildur Ísberg, Mr. Ingimar G. Haraldsson, Ms. Málfrídur Ómarsdóttir and Mr. Markús A.G. Wilde for their useful help during the training period. I am grateful to the UNU Fellows for the time we have had together.

Special thanks to my wife Dorcas M. Ndirangu for her support, love, encouragement, prayers and endurance during my stay in Iceland.

Thanks to Almighty God for giving me wisdom and the strength.

NOMENCLATURE

KNBS = Kenya National Bureau of Statistics;
MOA = Ministry of Agriculture;
EUSPA = European Union of swimming pool and spa associations;
GDC = Geothermal Development Company;
GDP = Gross Domestic Product;
FAO = Food and Agriculture Organisation;
NCPB = National Cereals and Produce Board; and
USD = US dollars.

REFERENCES

Breadley, R., Myers S., and Allen 2011: *Principles of corporate finance* (10th ed.). McGraw-Hill, Ltd., NY, 969 pp.

EPZA, 2005: *Grain production in Kenya 2005.* Export Processing Zone Authority, website: *www.epzakenya.com.*

EUSSA, 2010: *Domestic swimming pool water 2010*. European Union Swimming and Spa Association, website: *www.eusaswim.eu/Documentation/downloads/Paper-on-water-quality.pdf.*

FAO, 2008: *Basic principles of grain drying*. Food and Agriculture Organisation, website: *www.fao.org/home/en/*.

FAO, 2011: *Situation analysis: improving food safety in the maize value chain in Kenya*. Food and Agriculture Organisation, website: *www.fao.org/home/en/*.

GDC, 2013: *Well MW-03 discharge chemistry report.* Geothermal Development Company, Kenya, unpublished report, 12 pp.

Government of the Republic of Kenya, 2013: *Kenya Vision 2030*. Website: *www.vision2030.go.ke*

Halldórsson, G., 1975: *Heating and cleaning of water in swimming pools*. Sigurdur Thoroddsen Consulting Engineers, report ST 75 071 (in Icelandic), 63 pp.

Henderson, S.M., and Pabis, S., 1961: Grain drying theory I. Temperature effect on drying coefficient. *J. Agriculture Engineering Res., 6-3,* 169-174.

Jamieson, R.E., 1984: Simulation of the silica scaling process. *Proceedings of the 6th New Zealand Geothermal Workshop, Auckland University, Auckland, NZ,* 135-140.

Kashpur, V.N., and Popatov, V.V., 2000: Study of the amorphous silica scales formation at the Mutnovskoe hydrothermal field (Russia). *Proceedings of the 25th Workshop on Geothermal Reservoir Engineering Stanford University, Stanford, Ca,* 7 pp.

Kavak Akpinar, E., Bicer, Y., Cetinkaya, Y., 2006: Modelling of thin layer drying of parsley leaves in a convective dryer and under open sun. Research Gate, website: *www.reasearchgate.net.*

Kevin, D., Rafferty, P.E., and Gene, C., 1991: Heat exchangers. In: Lienau, P.J., and Lunis, B.C. (editors), *Geothermal direct use engineering and design guidebook*. Geo-Heat Centre, Institute of Technology, Klamath Falls, 247-261.

Kipng'ok, J.K., 2011: Fluid chemistry, feed zones and boiling in the first geothermal exploration well at Menengai, Kenya. Report 15 in: *Geothermal training in Iceland 2011*. UNU-GTP, Iceland, 281-302.

KNBS, 2012: *Maize production in Kenya.* Kenya Bureau of Statistics, website: *www.knbs.or.ke/.*

Kowalski, S.J., and Mierzwa, D., 2013: Numerical analysis of drying kinetics for shrinkable products such as fruits and vegetables. *J. Food Engineering*, 114-4, 522-529.

Lewis, W.K., 1921: The rate of drying of solid materials. *Ind. Eng. Chem., 13-5*, 427-432.

Liviu, G., and Badea, L., 2009: Aspects into the use of renewable energy sources in cereals drying process. *Proceedings of the 8th WSEAS International Conference on Signal Processing, Robotics and Automation 2009*, 74-77.

Maharjan R., 1995: Design of a dryer and a swimming pool using geothermal water. Report 7 in: *Geothermal training in Iceland 1995.* UNU-GTP, Iceland, 155-184.

Mangi P., 2012: Geothermal resource optimization: a case of the geothermal health spa and demonstration centre at the Olkaria geothermal project. *Presented at Short Course VII on Exploration*

*for Geothermal Resources, organized by UNU-GTP, GDC and KenGen, at Lake Bogoria and Lake Naivasha, Kenya,*10 pp.

MOA, 2001: *Grain growing areas in Kenya*. Ministry of Agriculture, Kenya.

Mwangi:, M., 2005: *Lectures on geothermal in Kenya and Africa*. UNU-GTP, Iceland, Report 4, 58 pp.

Ólafsson, J.H., and Sigurgeirsson, B., 2003: *The Blue Lagoon and psoriasis*. Blue Lagoon Ltd., 12 pp.

Orkustofnun, 2013: *Bathing and recreation*. Website: *www.nea.is/geothermal/direct-utilization /bathing--recreation.*

Panchariya, P.C., Popovic, D., and Sharma, A.L., 2002: Thin-layer modelling of black tea drying process. *J. Food Engineering, 52-4*, 349-357.

Perkins, P.H., 1988: *Swimming pools*. Elsevier Applied Science Publishers Ltd., London, 370 pp.

Pétursdóttir, S., and Kristjánsson, J.K., 1995: The relationship between physical and chemical conditions and low microbial diversity in the Blue Lagoon geothermal lake in Iceland. *FEMS Microbiology Ecology, 19-1,* 39-45.

RETScreen, 2011: *Retscreen international – Empowering cleaner energy decisions*. Natural Resources Canada, website: *http://www.retscreen.net/ang/home.php*

Ruiz, E., and Martınez, P.J., 2009: *Analysis of an open-air swimming pool solar heating system by using an experimentally validated TRNSYS model*. Universidad Miguel Hernandez, Edificio Torreblanca, Elche, Spain, 8 pp.

Shirbhate, D.V., 2013: *Design and study of grain dryer.* Scribd, website: *www.scribd.com/doc/7370568/Design-Study-of-Grain-Dryer,* 101 pp.

Sotocinal, A.S., 1992: *Design and testing of a natural convection solar fish dryer.* McGill University Montreal, Department of Agricultural Engineering, MSc thesis, 202 pp.

Temple S.J., Tambala S.T., and Boxtel A.J.B., 2000: Monitoring and control of fluid-bed drying of tea. *Control Engineering Practice, 8*, 165-173.

Tesha, 2006: Utilization of brine water for copra drying in Lahendong geothermal field, Indonesia. Report 20 in: *Geothermal training in Iceland 2006.* UNU-GTP, 453-470.

APPENDIX I: Results of variable distance transform for pipe route selection

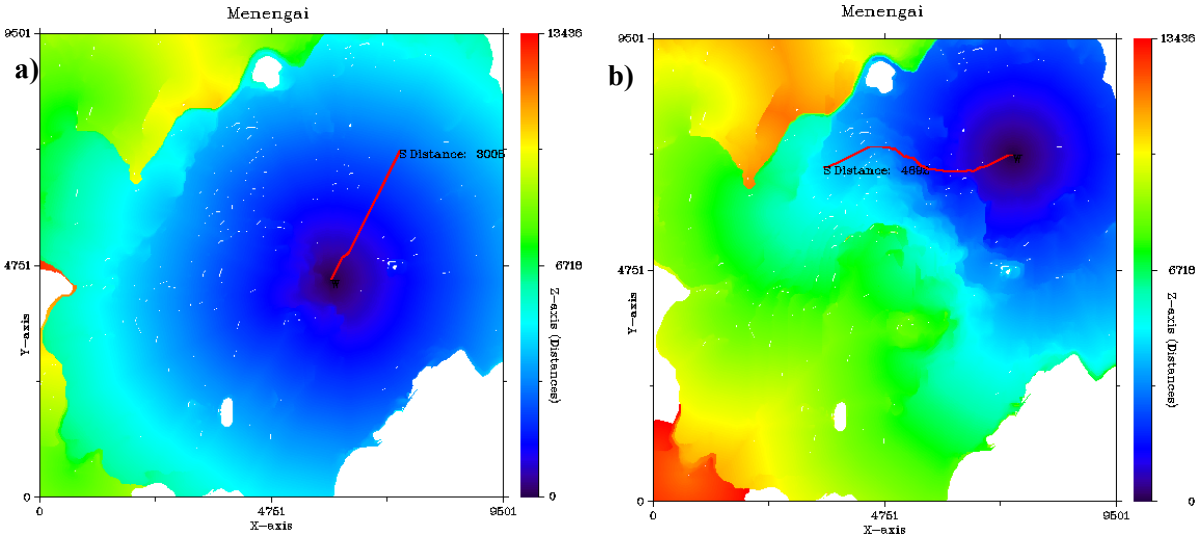

FIGURE 1: Map showing pipe route for supply (a) and re-injection (b) under scenario A

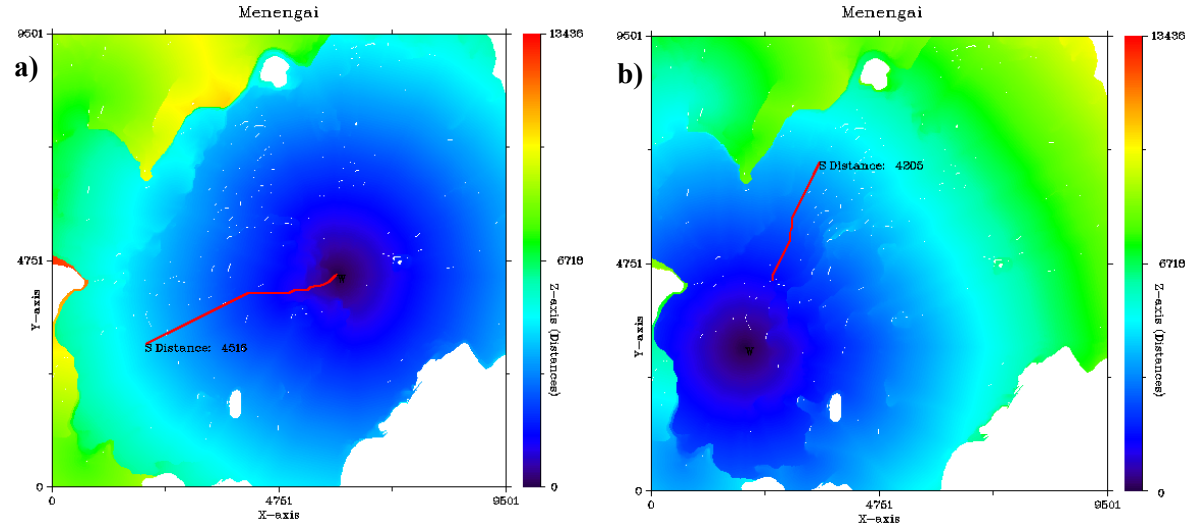

FIGURE 2: Map showing pipe route for supply (a) and re-injection (b) under scenario B

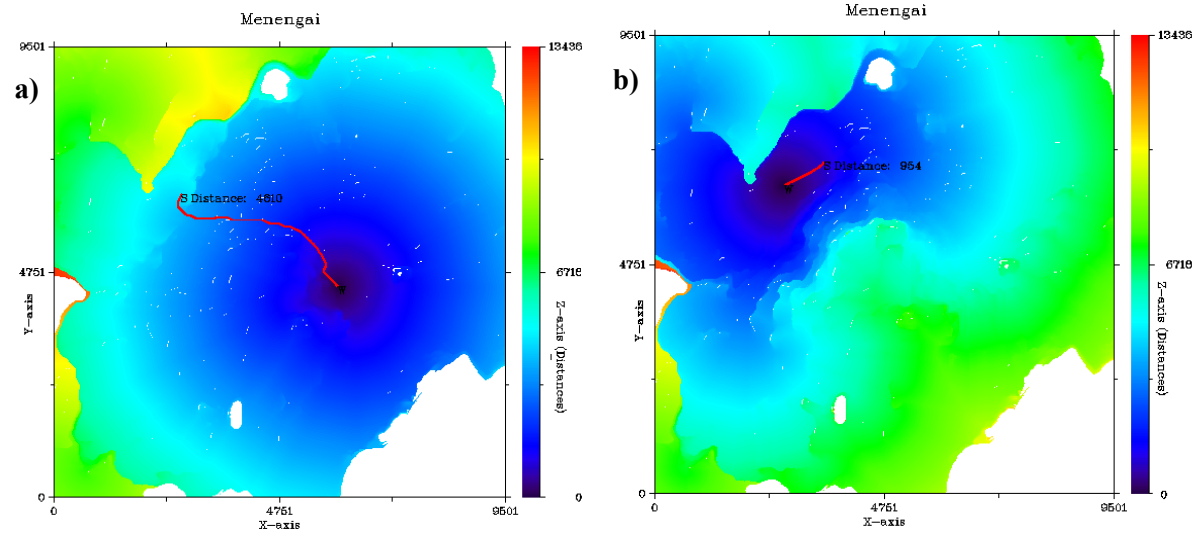

FIGURE 3: Map showing pipe route for supply (a) and re-injection (b) under scenario C

APPENDIX II: Shedd's curve showing resistance of grains to air flow

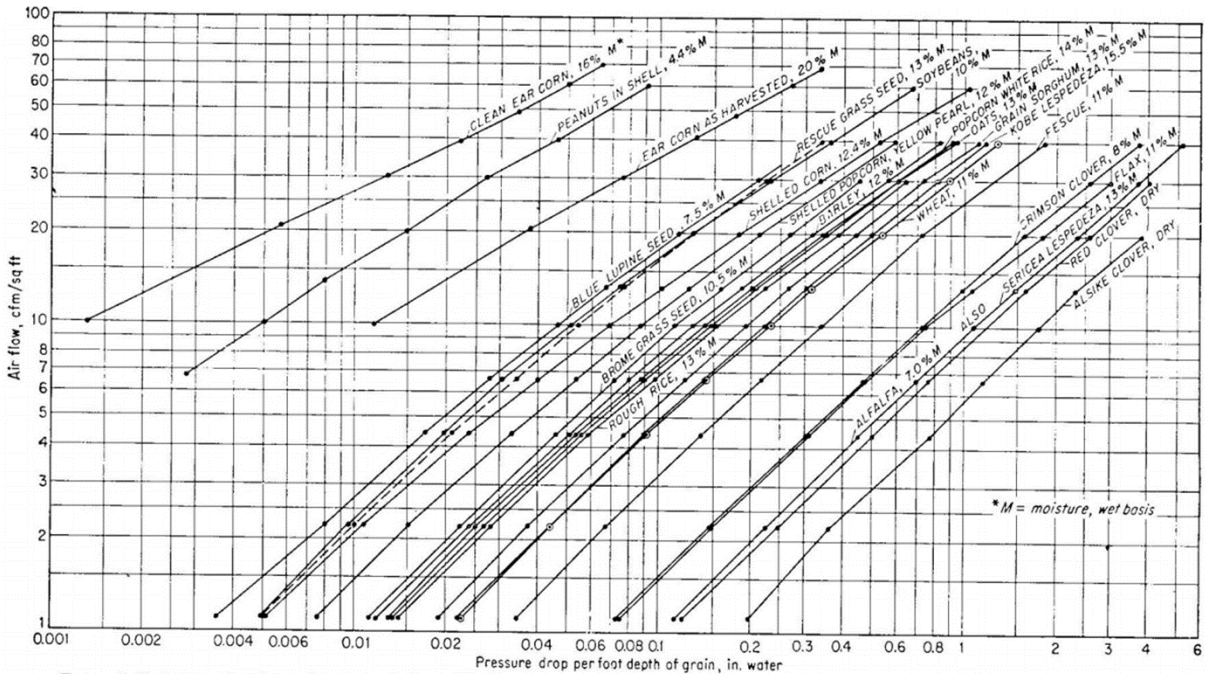

FIGURE 1: Resistance of grains to airflow (Shedd's characteristic curve, 1953)

APPENDIX III: Air properties during the drying process

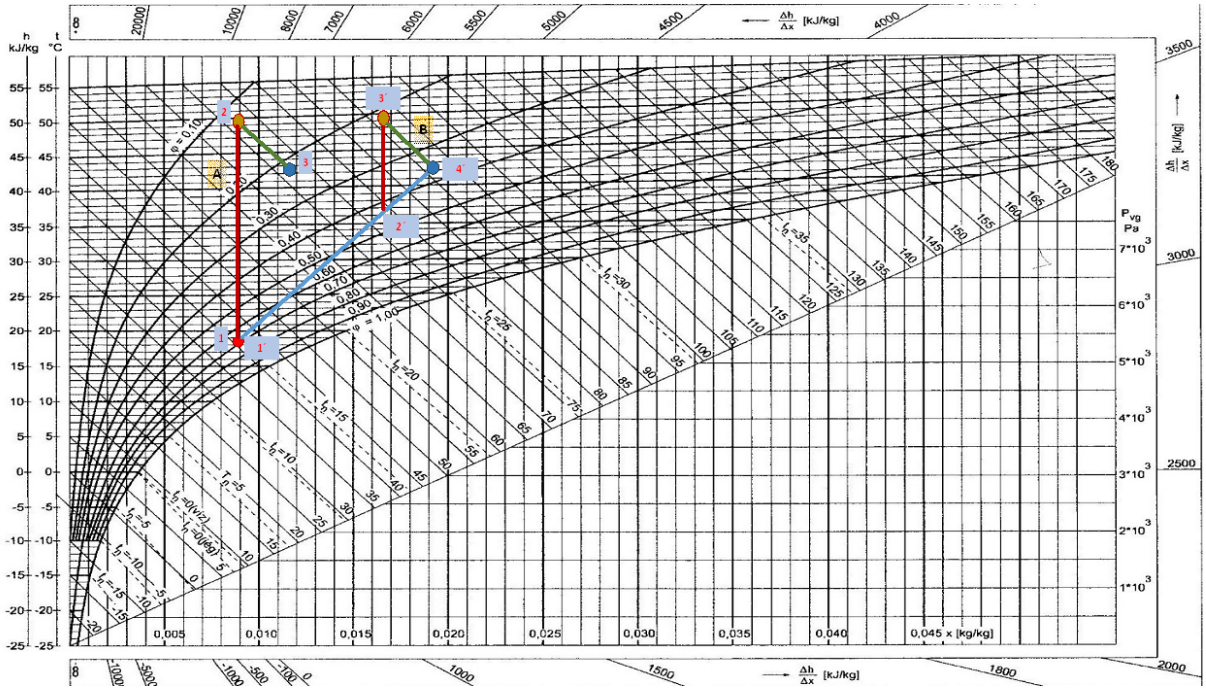

FIGURE 1: Psychometric chart indicating air properties under re-circulation